Supporting Information

Cu^{2+} Selective Chelators Relieve Copper-Induced Oxidative Stress *In Vivo*

Ananya Rakshit,[†] Kaustav Khatua,[†] Vinit Shanbhag,[‖] Peter Comba,[‡] and Ankona Datta*[†]

[†]Department of Chemical Sciences, Tata Institute of Fundamental Research, 1 Homi Bhabha Road, Colaba, Mumbai 400005, India.

[‖]Department of Biochemistry, Christopher S. Bond Life Science Center, University of Missouri, Columbia, United States.

[‡]Universität Heidelberg, Anorganisch-Chemisches Institut and Interdisciplinary Center for Scientific Computing, Heidelberg, Germany.

*Corresponding Author: Ankona Datta, Department of Chemical Sciences, Tata Institute of Fundamental Research, Mumbai 400005, India, Email: ankona@tifr.res.in

SUPPORTING INFORMATION

TABLE OF CONTENTS

1. General materials and methods

All chemicals were purchased from Sigma–Aldrich® or SD Fine-Chem Ltd. and used without further purification unless otherwise noted. All cell culture reagents were purchased from either Sigma-Aldrich® or Gibco®. Activated molecular sieves were used to dry methanol. Hydrogen peroxide (50 % w/w) was obtained from Fisher Scientific. Phen Green™ FL diacetate and CellROX® Deep Red reagent were obtained from Thermo Fisher Scientific. HEK293T cells were purchased from American Type Culture Collection (ATCC®). All primary and secondary antibodies were obtained from Sigma-Aldrich®. Protease inhibitor cocktail tablets were purchased from Roche Life Science. Water used for experiments was deionized using a Milli-Q® Integral 3 water purification unit (Millipore Corp. Billerica, MA, USA). Silica gel (230-400 mesh size, Merck & Co. Inc.) was used for column chromatography. Solvents used for separation were of analytical grade and used without distillation. Solvents were evaporated under reduced pressure using a rotary evaporator (BÜCHI Labortechnik AG). A Shimadzu Prominence UFLC system was used for HPLC purification of ligands. UV-Visible spectrophotometric measurement of ligands were performed on a double beam Perkin-Elmer (Lambda 750-UV/Vis/NIR) spectrophotometer in a 1 mL quartz cuvette having a path length of 1 cm. ^{1}H NMR and ^{13}C NMR spectra were collected in either $CDCl_3$ or CD_3OD as a solvent (Cambridge Isotope Laboratories, Cambridge, MA) at 25 °C on a Varian 600 MHz spectrometer at the National NMR facility, Tata Institute of Fundamental Research, Mumbai, India. All chemical shifts are reported in the standard notation of parts per million (ppm) using the peaks of proton signals of residual solvents for calibration. The abbreviations used for the proton spectra multiplicities are: s, singlet; bs, broad singlet; d, doublet; t, triplet; m, multiplet. Liquid chromatography mass spectrometry (LCMS) analyses were carried out on a Shimadzu LCMS 2020 with an ESI probe (positive and negative ion modes). High-resolution mass spectrometry analyses were carried out at the Chemistry Department, Indian Institute of Technology, Bombay, India on a maXisTM impact ESI-qTOF mass spectrometer (Bruker Corp.). Electron paramagnetic resonance (EPR) was carried out in a Bruker EMX-Micro X-band EPR spectrophotometer. EPR simulation was performed using SimFonia software. For cell viability experiments a Tecan Infinite® M200 PRO microplate reader was used for measuring absorbance at 570 nm in a 96 well plate.

For all measurements, stock solutions of ligands **2c** and **3c** were prepared in dimethyl sulfoxide (DMSO) and stored at -10 °C. Stock solutions were then diluted in appropriate aqueous buffer and care was taken such that the percentages of DMSO never exceeded 5 % in each experiment. Exact percentage of DMSO and buffers used have been mentioned in the figure captions.

Zebrafish were bred and maintained and experiments were performed in accordance with guidelines and protocols approved by the institutional animal ethics committee of the Tata Institute of Fundamental Research.

2. Synthetic procedures for chelators

Synthesis of 1: Compound **1** was synthesized according to a previously reported procedure.[1]

Synthesis of 2b: Compound **2b** was synthesized via a modified procedure than previously reported.[2] A solution of **1** (0.1 g, 0.56 mmol) in degassed sodium acetate buffer (0.1 M, pH 4.5) was transferred to a three-neck round-bottom flask under argon atmosphere. The mixture was degassed by applying vacuum and argon alternately and then heated to 100 °C. A solution of salicylaldehyde (0.3 g, 2.5 mmol) in anhydrous methanol was added dropwise to the reaction mixture and refluxed for 19 h. A brown gummy precipitate formed with the progress of the reaction. The reaction was followed by checking the ESI-MS spectra of the reaction mixture. After completion of the reaction, the mixture was extracted in dichloromethane and washed with water. The organic layer was dried over sodium sulfate, filtered and evaporated under reduced pressure. Compound **2b** was left for drying under vacuum for 2 days after which a brown solid was obtained (0.202 g, 93 % yield). ^{1}H NMR (600 MHz, $CDCl_3$) δ 13.26 (bs, 2H), 8.21 (s, 2H), 7.21-7.26 (m, 5H), 7.15 (d, *J* = 7.2, 2H), 6.96 (d, *J* = 7.8, 2H), 6.85 (t, *J* = 7.2, 2H), 6.77-6.76 (m, 2H), 3.77 (t, *J* = 5.4, 4H), 3.70 (t, *J* = 5.4, 4H). ^{13}C NMR (150 MHz, $CDCl_3$): δ 161.24, 155.84, 141.67, 127.13, 126.15, 124.35, 113.51, 113.41, 111.77, 111.58, 107.18, 51.93, 47.53. HR-MS (ESI): m/z observed 388.2028 $[M+H]^+$, calculated 388.2020 for $C_{24}H_{25}N_3O_2$.

Synthesis of 3b: Compound **3b** was synthesized using the same procedure as that of **2b**. A solution of **1** (0.023 g, 0.13 mmol) was taken in degassed sodium acetate buffer (0.1 M, pH 4.5). 2-hydroxy-5-methoxybenzaldehyde (0.048 g, 0.39 mmol) in anhydrous methanol was added dropwise to the mixture and the mixture was heated to 90 °C. The reaction mixture immediately turned turbid yellow upon addition of the aldehyde. The reaction mixture was refluxed for 4 h. After completion of the reaction, the mixture was extracted in dichloromethane and washed with water. The organic layer was dried over sodium sulfate, filtered and evaporated under reduced pressure. The mixture was purified by column chromatography on silica gel (4 % methanol in dichloromethane) to afford **3b** as a yellowish gummy solid (0.031 g, 54 % yield).

^{1}H NMR (600 MHz, $CDCl_3$): δ 12.77 (bs, 2H), 8.16 (s, 2H), 7.27 (t, *J* = 7.8, 1H, $CHCl_3$, 1H), 6.92-6.89 (m, 4H), 6.77- 6.73 (m, 4H), 6.67-6.66 (m, 2H), 3.77 (t, *J* = 6.0, 4H), 3.75 (s, 6H), 3.69 (t, *J* = 6.0, 4H). ^{13}C NMR (150 MHz, $CDCl_3$): δ 160.96, 149.96, 146.80, 141.71, 124.35, 114.20, 113.16, 112.50, 111.58, 109.65, 107.15, 52.05, 50.69, 47.53. HR-MS (ESI): m/z observed 448.2235 $[M+H]^+$ calculated 448.2231 for $C_{26}H_{29}N_3O_4$.

Synthesis of 2c: A solution of **2b** (0.097 g, 0.25 mmol) in anhydrous methanol was transferred into a three-neck round-bottom flask under argon atmosphere. The solution was degassed twice and cooled

to 0 °C. Solid sodium borohydride (0.076 g, 2.0 mmol) was added to the flask under argon atmosphere. The mixture was stirred for 2 h. The reaction was monitored using ESI-MS. After 2 h, the reaction was quenched with dilute hydrochloric acid and dried under reduced pressure. The isolated crude product was purified via HPLC and **2c** was obtained as a brown solid (0.076 g, 77 % yield). ^{1}H NMR (600 MHz, CD_3OD): δ 7.29-7.26 (m, 6H), 6.94 (d, *J* = 8.4, 2H), 6.90-6.88 (m, 5H), 4.22 (s, 4H), 3.66 (t, *J* = 6.6, 4H), 3.16 (t, *J* = 6.6, 4H). ^{13}C NMR (150 MHz, $CDCl_3$): δ 156.88, 149.77, 139.94, 126.63, 125.65, 125.27, 123.53, 121.35, 115.72, 111.48, 49.02, 44.72, 39.63. HR-MS (ESI): m/z observed 392.2340 $[M+H]^+$, calculated 392.2333 for $C_{24}H_{30}N_3O_2$.

Synthesis of 3c: Compound **3c** was synthesized using the same procedure as that of **2c**. Compound **3b** (0.050 g, 0.11 mmol) was used for the reaction. The isolated crude product was purified via HPLC and **3c** was obtained as a brown solid (0.028 g, 57 % yield). ^{1}H NMR (600 MHz, CD_3OD): δ 7.32 (t, *J* = 7.8, 2H), 6.98 (d, *J* = 8.4, 2H), 6.94 (t, *J* = 7.2, 1H), 6.91-6.89 (m, 4H), 6.85 (d, *J* = 8.4, 2H), 4.22 (s, 4H), 3.76 (s, 6H), 3.68 (t, *J* = 7.2, 4H), 3.19 (t, *J* = 7.2, 4H). ^{13}C NMR (150 MHz, $CDCl_3$): δ 148.38, 143.48, 140.03, 125.66, 123.50, 121.38, 112.40, 112.02, 111.90, 110.09, 50.53, 49.02, 44.78, 39.69. HR-MS (ESI): m/z observed 452.2548 $[M+H]^+$, calculated 452.2544 for $C_{26}H_{34}N_3O_4$.

Synthesis of 2-((benzylamino)methyl)phenol: 2-((benzylamino)methyl)phenol was synthesized following a reported procedure.[3] The isolated crude product was purified via HPLC.

3. HPLC column conditions for purification of ligands 2c and 3c

Chelators **2c**, and **3c** were purified on a Phenomenex Luna® C18(2) (5 µm, 10 × 250 mm) semi preparative column using a linear 70 min gradient from 5 % solvent B in A to 100 % solvent B in A at a flow rate of 2 mL/min where solvent A was water with 0.1 % (v/v) trifluoroacetic acid and solvent B was acetonitrile with 0.1 % (v/v) trifluoroacetic acid.

4. Purity analysis of ligands

LC-MS of 2b and 3b

A Phenomenex Luna® C18(2) (5 µm, 4.6 mm × 150 mm) column and a linear 60 min gradient from 10 % solvent B in A to 100 % solvent B in A (solvent A was 1 : 9 water : methanol with 1 mM ammonium acetate and solvent B was 1 : 9 water : acetonitrile with 1 mM ammonium acetate) with a flow rate of 0.2 mL/min was used for purity analysis.

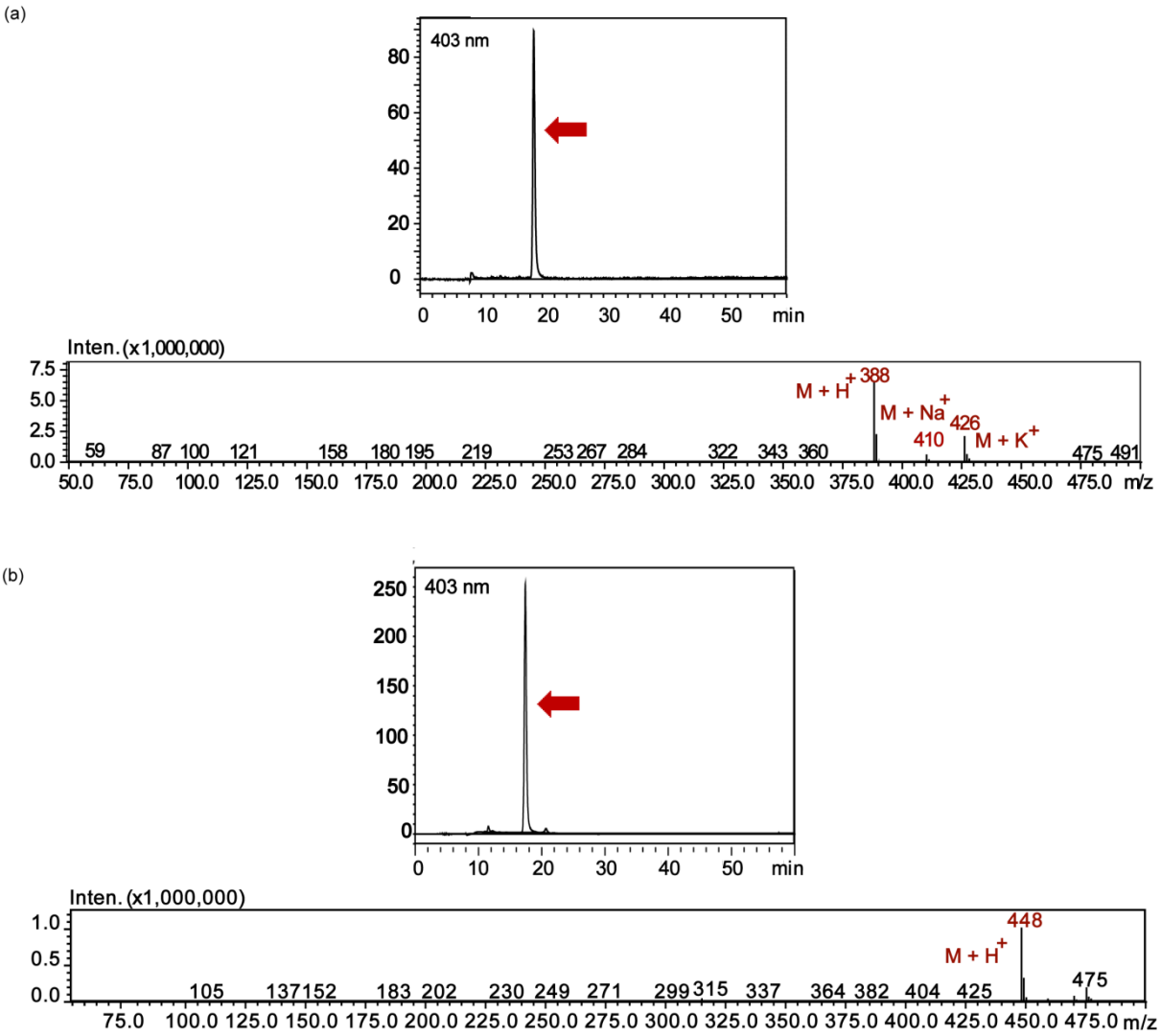

Fig. S1. LC-ESI-MS of ligand (a) **2b** and (b) **3b** confirming sample purity (LC depicting absorption intensity at 403 nm). The major elution peak is pointed with a red arrow and the corresponding ESI-MS trace in the positive mode shows the mass of the compound, highlighted in red.

LC-MS of 2c and 3c

An Agilent C18 (5 µm, 4.6 mm × 250 mm) column and a linear 60 min gradient from 10 % solvent B in A to 100 % solvent B in A (solvent A was water with 0.01 % (v/v) formic acid and solvent B was acetonitrile with 0.01 % (v/v) formic acid) with a flow rate of 0.2 mL/min was used for purity analysis.

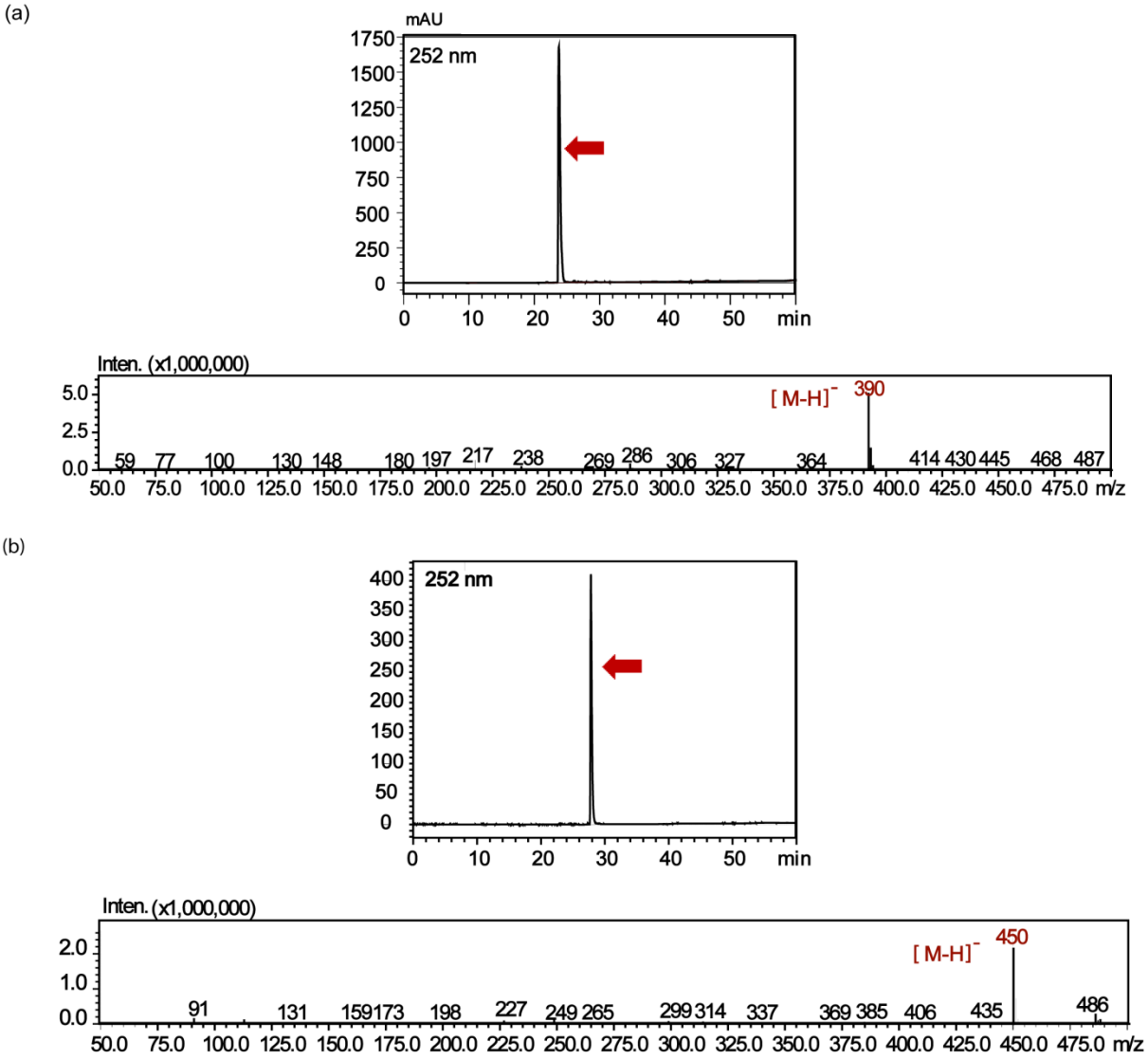

Fig. S2. LC-ESI-MS for ligand (a) **2c**, and (b) **3c** confirming sample purity (LC depicting absorption intensity at 252 nm). The major elution peak is pointed with a red arrow and the corresponding ESI-MS in the negative mode shows the mass of the compound, highlighted in red.

5. Stability of ligands in solution

At different time intervals (0 min, 30 min, 1 h, 2 h, 4 h, 6 h, 8 h, 10 h, and 12 h), solutions of ligand (stock solutions in DMSO) were diluted in solvent (final volume 500 µL), injected into the column and the stability of the ligand was monitored over time. Solutions of **2c** and **3c** were prepared in HEPES buffer where final solvent composition was 0.6 % DMSO in buffer. Stabilities of **2c** and **3c** were also checked in Dulbecco's Modified Eagle's Medium-F12 (DMEM) with 1 % penicillin and streptomycin buffered to pH 7.2.

An Agilent C18 column (5 µm, 4.6 mm × 250 mm) was used to monitor the stability of ligands **2c** and **3c**. In all cases, a linear gradient from 10 % solvent B in A to 100 % solvent B in A was run at 0.2

mL/min for 60 min. The eluting solvents used for each analysis are listed in Table S1. Liquid chromatography traces were integrated to obtain percentage of ligands.

Table S1. Eluting solvents used for determination of ligand stability in solutions.

Ligand	Mobile phase composition		Wavelength monitored in LC (nm)
	Solvent A	Solvent B	
2c	water with 0.01 % (v/v) formic acid	acetonitrile with 0.01% (v/v) formic acid	250
3c	water with 0.01 % (v/v) formic acid	acetonitrile with 0.01% (v/v) formic acid	310

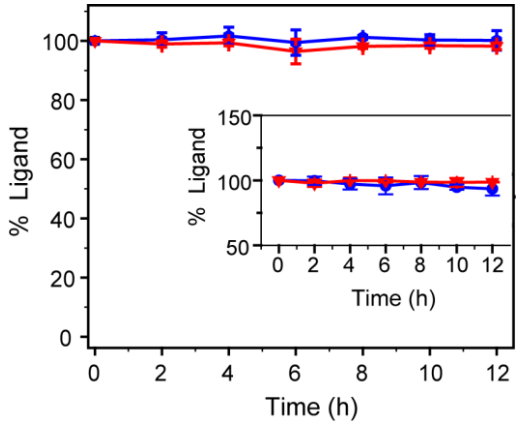

Fig. S3. Stability of ligands in aqueous media. Percentage of **2c** (red triangles) and **3c** (blue hexagons) in HEPES buffer were followed with time using LC-ESI-MS. The inset shows stability data for **2c** (red triangles) and **3c** (blue hexagons) in Dulbecco's modified Eagle's medium (DMEM).

6. Absorbance measurements

Unless mentioned, all spectroscopic measurements were performed in 20 mM HEPES buffer (100 mM NaCl, pH 7.0) at room temperature. $Cu^{2+}$and Co^{2+} ions were delivered in the form of $CuCl_2$, and $CoCl_2$, respectively from stock solutions (10 mM) in water. Ni^{2+}, Ca^{2+}, and Mn^{2+} were delivered as $NiCl_2$, $CaCl_2.2H_2O$, and $MnCl_2.4H_2O$, respectively from stock solutions (10 mM) prepared in HEPES buffer. Zn^{2+} was supplied as $ZnCl_2$ from a stock solution (5 mM) in HEPES buffer. Fe^{3+} was delivered in the form of $FeCl_3.6H_2O$ from a freshly prepared stock solution (2.5 mM) in water. Fe^{2+} was

delivered in the form of $(NH_4)_2SO_4FeSO_4.6H_2O$ from a freshly prepared stock solution (1 mM) in deoxygenated water. Cu^+ was supplied as tetrakis(acetonitrile)copper(I) hexafluorophosphate from a stock solution (2.5 mM) prepared in degassed aqueous ascorbic acid solution (4 mM).

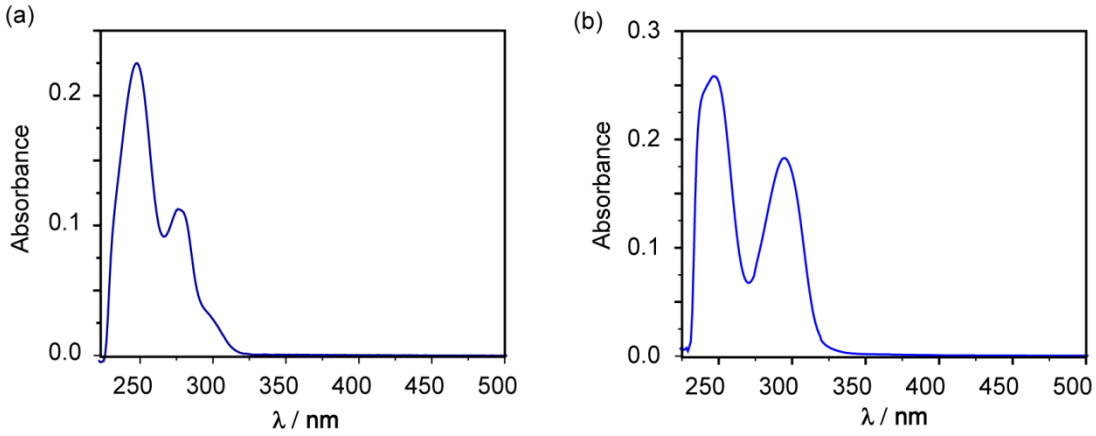

Fig. S4. UV-visible spectra of chelators (50 µM). (a) Chelator **2c** and (b) chelator **3c** in HEPES buffer. Final composition of the solvent was 0.2 % DMSO in HEPES buffer (100 mM NaCl, pH 7.0).

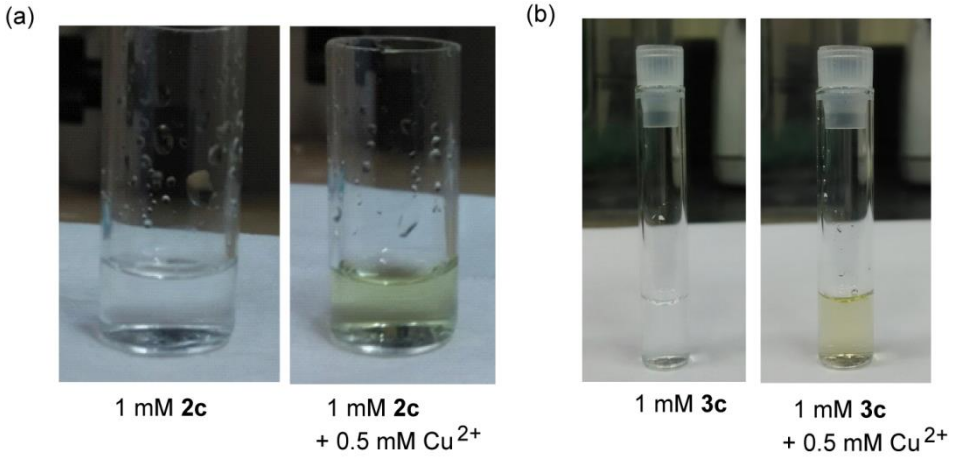

Fig. S5. Colorimetric response of chelators in presence of $CuCl_2$. Glass vials containing chelator (1 mM) and chelator with Cu^{2+} (0.5 mM). (a) Left: Chelator **2c** (colorless), right: Chelator **2c** with Cu^{2+} (light green); (b) left: Chelator **3c** (colorless), right: Chelator **3c** with Cu^{2+} (light green) in HEPES buffer. Final composition of the solvent was 4 % DMSO in HEPES buffer (100 mM NaCl, pH 7.0).

Table S2. Extinction coefficient (ε_λ) of chelators 2c, 3c and their corresponding Cu^{2+} complexes.

Compounds	**2c**	**3c**	**Cu^{2+} : 2c (1 : 2) Complex**	**Cu^{2+} : 3c (1 : 2) Complex**
Extinction Coefficient ε (λ nm) M^{-1} cm^{-1}	5210 (247 nm) 2660 (277 nm) 551 (302 nm)	5330 (247 nm) 3780 (295 nm)	736 (420 nm) 173 (623 nm)	832 (450 nm) 275 (626 nm)

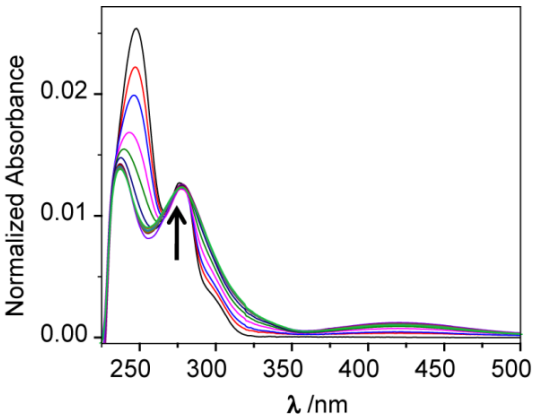

Fig. S6. Normalized absorbance spectra of chelator **2c** (50 µM) with increasing concentrations of Cu^{2+} (0-60 µM) in HEPES buffer. Final composition of the solvent was 0.2 % DMSO in HEPES buffer (100 mM NaCl, pH 7.0). Black arrow is pointing toward the isosbestic point in the absorbance spectra.

Job's plot

To determine the binding stoichiometry of chelator to Cu^{2+}, Job's continuous variation method was employed using absorbance spectroscopy. Chelators were added from 10 mM stock solutions in DMSO and Cu^{2+} was added from a 3 mM stock solution in water. The absorbance signal was recorded for solutions where concentration of both chelator and Cu^{2+} were varied while the sum of their concentrations was kept constant (300 µM). Final composition of solvent in each solution was 0.3 % DMSO in HEPES buffer. After equilibrating for 2 h, the absorbance spectrum of each solution was recorded at 25 °C. Absorbance at a particular wavelength was plotted as a function of the mole fraction of the chelator. The maximum point in the resulting plot corresponds to the mole fraction of bound Cu^{2+} in the complex. Job's plots for Cu^{2+}-**2c** and Cu^{2+}-**3c** are shown in Fig. S7 and Fig. 3d, respectively.

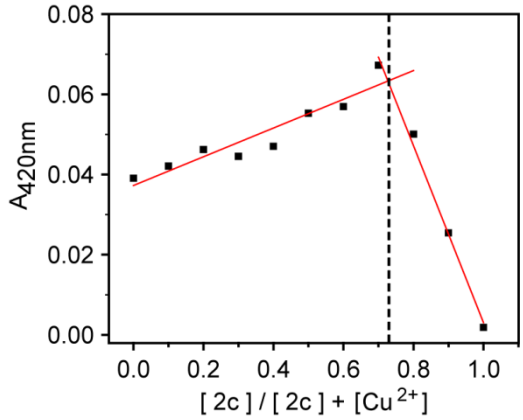

Fig. S7. Job's plot for Cu^{2+}-**2c** system. Absorbance at 420 nm was plotted as a function of molar ratio of **2c**. Scatter plots were fitted to linear equations where red lines denote the fitted plots. The crossing point at 0.71 indicated a 1: 2 stoichiometry of Cu^{2+}: **2c** complex.

7. ESI-MS of Cu^{2+} complexes

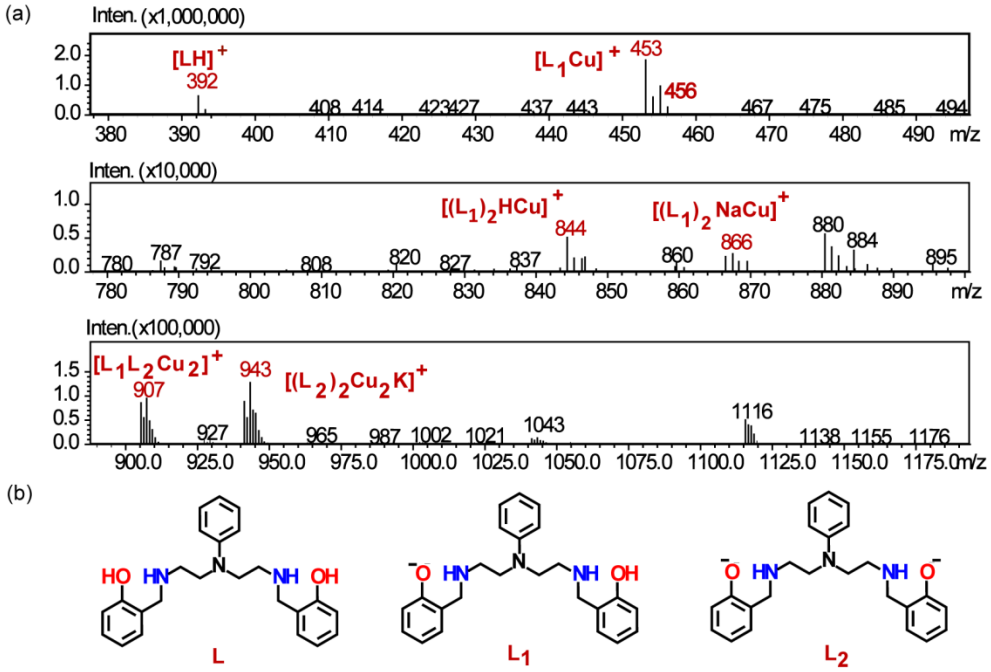

Fig. S8. Characterization of Cu^{2+}-**2c** complexes by ESI-MS. (a) ESI-MS trace of chelator **2c** (50 µM) with $CuCl_2$ (25 µM) in methanol showing the mass of different Cu^{2+}-**2c** complexes in the positive mode, highlighted in red. (b) Possible speciation of chelator **2c** that can form Cu^{2+}-**2c** complexes.

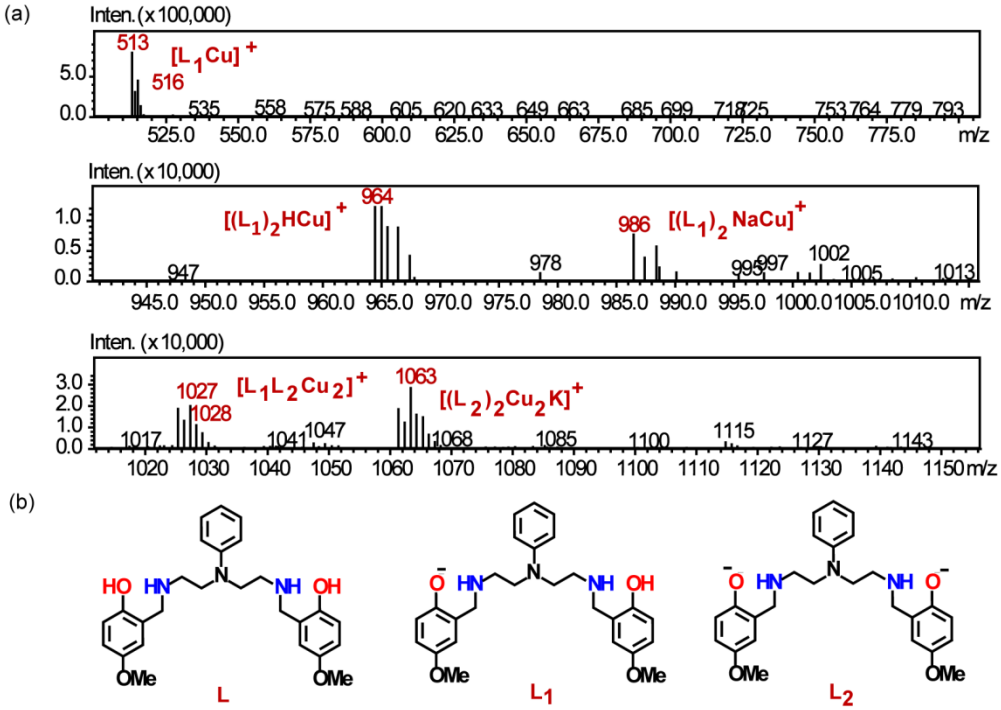

Fig. S9. Characterization of Cu^{2+}-**3c** complexes by ESI-MS. (a) ESI-MS trace of chelator **3c** (50 µM) with $CuCl_2$ (25 µM) in methanol showing the mass of different Cu^{2+}-**3c** complexes in positive mode, highlighted in red. (b) Possible speciation of chelator **3c** that can form Cu^{2+}-**3c** complex.

8. Equations for determining conditional stability constants (β) of the ligands to metal ions

Binding affinity of chelators to Cu^{+}, Fe^{2+}, Ni^{2+}, Zn^{2+}, Mn^{2+}, and Co^{2+}

Considering a 1:1 metal: ligand binding model, dissociation constant (K_d) was determined from a plot of observed absorbance intensity (A) at any particular wavelength versus $[M^{n+}]$ and the data was fitted to either equation (1) or equation (2).

$$K_d = \frac{(A_{max} - A_0)}{(A - A_0)} [M^{n+}] \quad \cdots\cdots\cdots (1)$$

Where A is the observed absorbance, A_{max} is the absorbance of ML complex and A_0 is the absorbance intensity of the ligand in absence of any metal ion.

$$K_d = \frac{(A - A_{min})}{(A_0 - A)} [M^{n+}] \cdots\cdots\cdots (2)$$

Where A is the observed absorbance, A_{min} is the absorbance of ML complex and A_0 is the absorbance intensity of the ligand in absence of any metal ion.

The stability constant for any metal-ligand complex was obtained from equation 3.

$$\beta = \frac{1}{K_d} \ldots\ldots\ldots (3)$$

Absorbance response of chelator to different metal ions was fitted to the binding model using either OriginPro2015 or DynaFit version 4 software.

Cu^{2+} stability constant

The absorption isotherms and the Job's plots indicated 1:2 Cu^{2+}: ligand complexes for **2c** and **3c**. Hence, in order to obtain the stability constants for Cu^{2+} with the chelators, we have considered a 1: 2 binding model for metal (M) and ligand (L). The overall stability constant (β) for a ligand-metal complex can be expressed as shown in equation (4).

$$\beta_{12} = \frac{[ML_2]}{[M]\,[L]^2} \quad \cdots\cdots\cdots (4)$$

$$M_0 = M + ML_2 \quad \cdots\cdots\cdots (5)$$

$$L_0 = L + 2ML_2 \quad \cdots\cdots\cdots (6)$$

$$A_{max} = \epsilon.[ML_2] \quad \cdots\cdots (7)$$

M_0 and L_0 are the total concentrations of metal ion and ligand, respectively. M and L represent free metal and free ligand. We calculated $\epsilon_{420\ nm}$ and $\epsilon_{450\ nm}$ of ML_2 complexes for chelators **2c** and **3c**, respectively, from the binding saturation points in the absorption isotherms. Using equation (5) and (6), equation (4) can be re-written as follows:

$$4[ML_2]^3 - 4[ML_2]^2([L_0] + [M_0]) + [ML_2]([L_0]^2 + 4[M_0][L_0] + \frac{1}{\beta_{12}}) - [M_0]\,[L_0]^2 = 0 \qquad \cdots (8)$$

For any given β_{12} value, $[ML_2]$ was calculated from equation (8).

We then obtained A_{sim} (absorbance at a specific wavelength at a given concentration of ligand L_0) by plugging in, ϵ and $[ML_2]$ values obtained from equations (7) and (8) respectively, to equation (9).

$$A_{sim} = \epsilon.[ML_2] \quad \cdots\cdots\cdots (9)$$

The simulated absorbance data was compared with the experimental data to determine the lower limit of stability constants for binding of chelators to Cu^{2+}.

Fe^{3+} binding affinity

The binding affinity of ligands to Fe^{3+} was measured via constant volume absorption titrations (Fig. S15a and b). In a constant volume experiment (final volume 0.5 mL), ligand (50 µM) and $FeCl_3.6H_2O$ (0-250 µM) were added in HEPES buffer and allowed to equilibrate for 10 mins. Another set of titrations were performed in the absence of ligands. $FeCl_3$ has an intense broad absorption band ranging from 200 nm to 450 nm and the $FeCl_3$ absorption features at 350 nm dominate the chelator titration spectra (Fig. S15a and S15b). A decrease in the absorbance of $FeCl_3$ at 350 nm was observed in the presence of chelators (Fig. S15c). If we assume that the absorbance at 350 nm is only due to unbound Fe^{3+} then concentration of free Fe^{3+} ions can be calculated from the extinction coefficient of $FeCl_3.6H_2O$ ($\varepsilon_{350\ nm}$ = 1400 $M^{-1}cm^{-1}$). Since the total concentration of ligand is known, for each titration point, the concentration of metal-ligand (ML) complex and L_{free} can be calculated. For each set of absorption spectrum in the titration experiments, M_{free}, L_{free}, and ML can be calculated using a 1:1 metal: ligand binding model. Dissociation constant K_d can be written as,

$$K_d = \frac{[M_{free}]\,[L_{free}]}{[ML]} \quad \cdots\cdots\cdots (10)$$

Using equation (10), if $[M_{free}][L_{free}]$ is plotted against [ML], then from the slope of the linear plot, K_d

can be calculated. Hence, equation (10) was used to determine the K_d values for Fe^{3+} with the ligands (Fig. S15d). The stability constant (β) values were obtained from equation (3).

9. Plots for stability constant determination and competition experiments

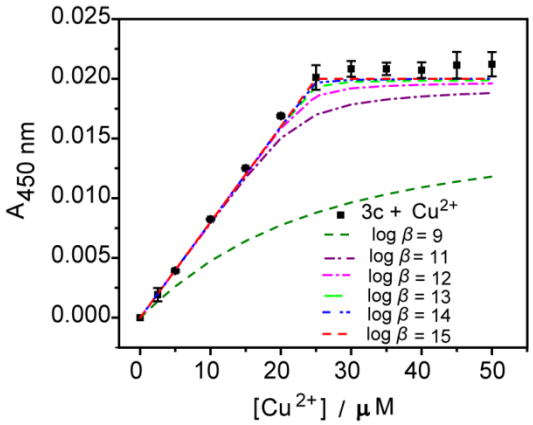

Fig. S10. Absorption binding plot for titration of Cu^{2+} to **3c** (50 μM) with simulated fits (fitted to the equation: $\beta = [ML_2] / [M][L]^2$ for different values of log β).

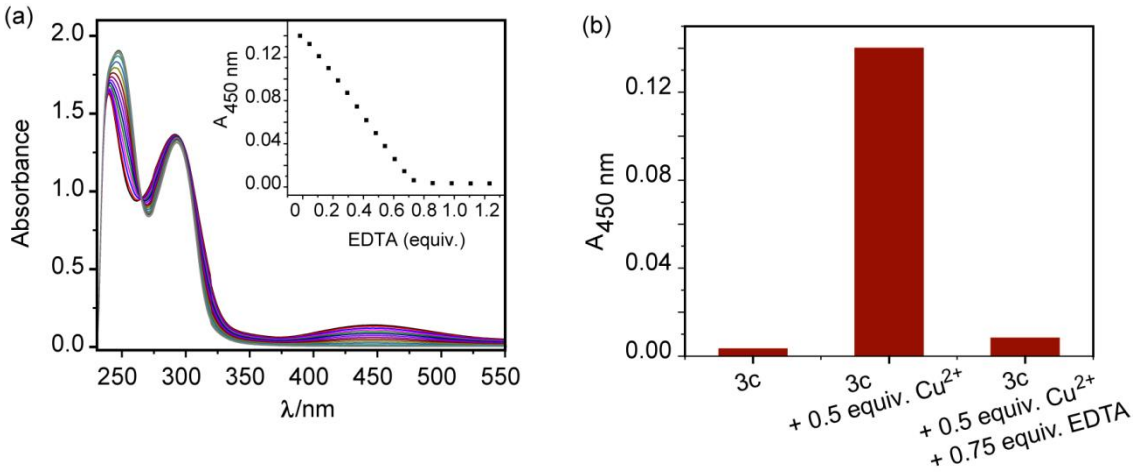

Fig. S11. Competition titration between Cu^{2+}-**3c** complex and EDTA. (a) Absorbance spectra of chelator **3c** (400 μM) with Cu^{2+} (200 μM), upon titrating with EDTA (0-700 μM) in HEPES buffer. Final composition of the solvent was 1.6 % DMSO in HEPES buffer (100 mM NaCl, pH 7.0). Inset: Absorbance at 450 nm was plotted with the equivalents of EDTA added. (b) Bar plot representing the absorbance intensities at 450 nm.

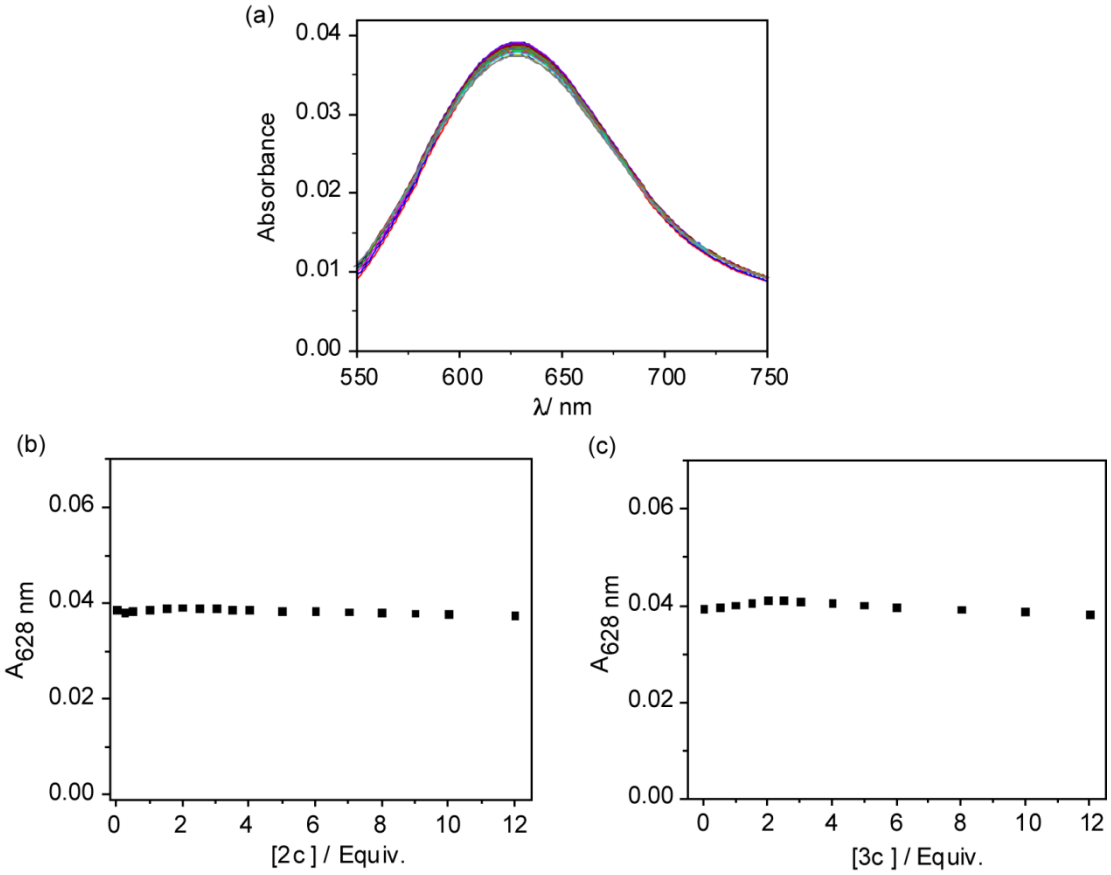

Fig. S12. Competition titration between Cu^{2+}-azurin complex (10 µM) and chelators. Absorbance titration spectra of (a) Cu^{2+}-azurin complex with increasing concentrations of chelator **2c** (0-120 µM). (b) Plot of absorbance at 628 nm with increasing equivalents of **2c** (0-12 equivalent); (c) Plot of absorbance at 628 nm with increasing equivalents of the chelator **3c** (0-12 equivalent) in HEPES buffer. Final composition of the solvent was 0.5 % DMSO in HEPES buffer (100 mM NaCl, pH 7.0).

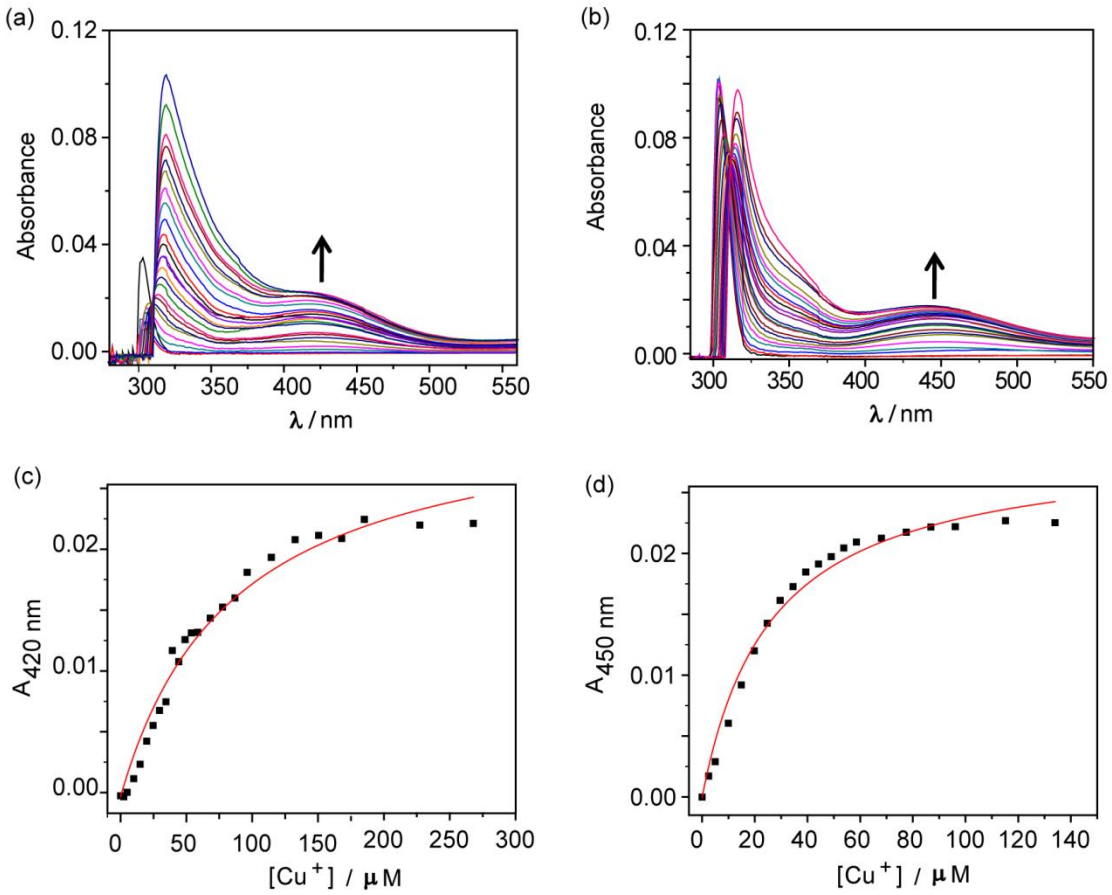

Fig. S13. Absorption titration spectra of chelators (50 μM) with increasing concentrations of $[Cu(CH_3CN)_4]PF_6$. (a) Chelator **2c** with Cu^+ (0-300 μM); (b) Chelator **3c** with Cu^+ (0-300 μM) in degassed HEPES buffer. Final composition of the solvent was 0.2 % DMSO in HEPES buffer (100 mM NaCl, pH 7.0). Absorbance at a specific wavelength was plotted against the concentration of Cu^+ for (c) **2c** and (d) **3c**. The absorbance response was fitted to equation (1). The red lines represent the fits. Arrows represent increase in absorbance intensity upon addition of metal ions.

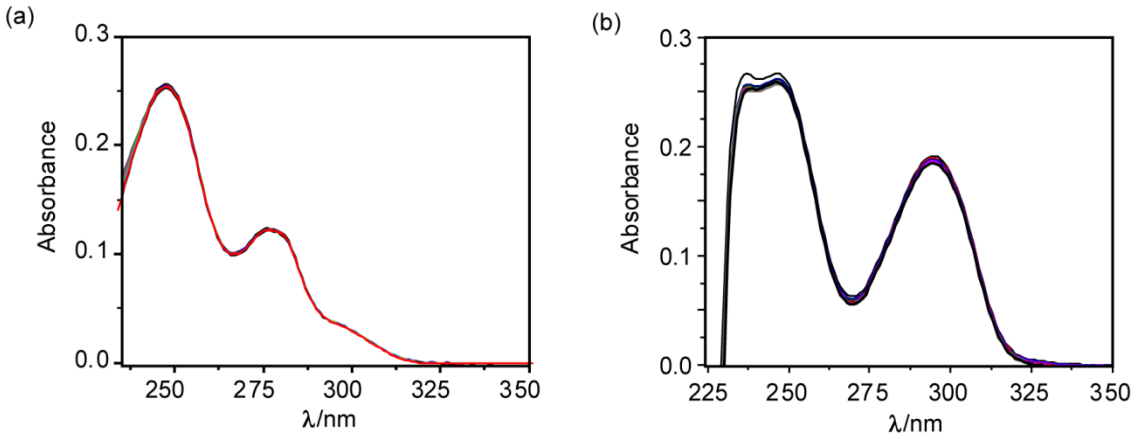

Fig. S14. Absorption titration spectra of chelators (50 μM) with $CaCl_2.2H_2O$. (a) Chelator **2c** with Ca^{2+} (0-1 mM); (b) Chelator **3c** with Ca^{2+} (0-1 mM). Final composition of the solvent was 0.2 % DMSO in HEPES buffer (100 mM NaCl, pH 7.0).

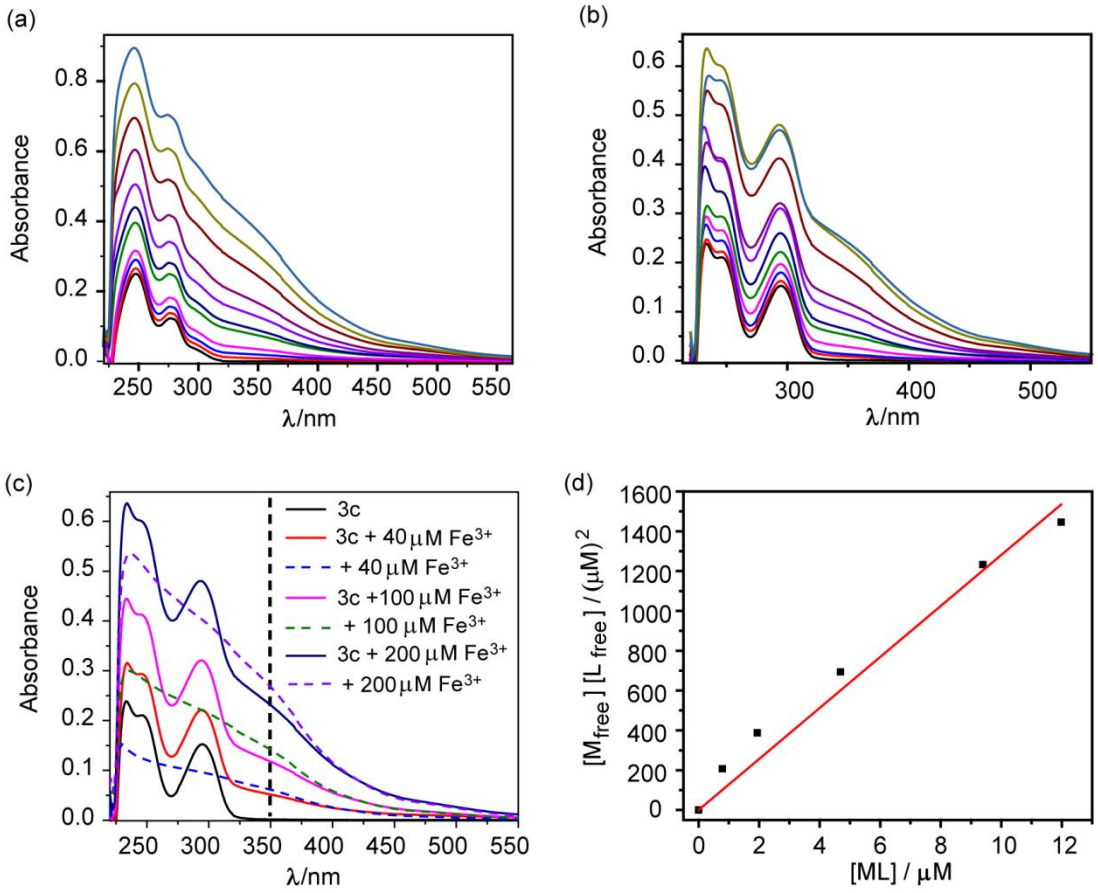

Fig. S15. Absorption titration spectra of chelators (50 μM) with increasing concentrations of $FeCl_3$. $6H_2O$. (a) Chelator **2c** with Fe^{3+} (0-250 μM); (b) Chelator **3c** with Fe^{3+} (0-250 μM) in HEPES buffer. Final composition of the solvent was 0.2 % DMSO in HEPES buffer (100 mM NaCl, pH 7.0). **(**c) Overlaid absorbance spectra of $FeCl_3.6H_2O$ with chelator **3c** (solid line) and without **3c** (dashed line). Black line indicates the absorbance at 350 nm. (d) Plot of $[M_{free}]$ $[L_{free}]$ versus [ML] for chelator **3c.** The plot was fitted to equation (10) and β was calculated from the slope of the linear plot.

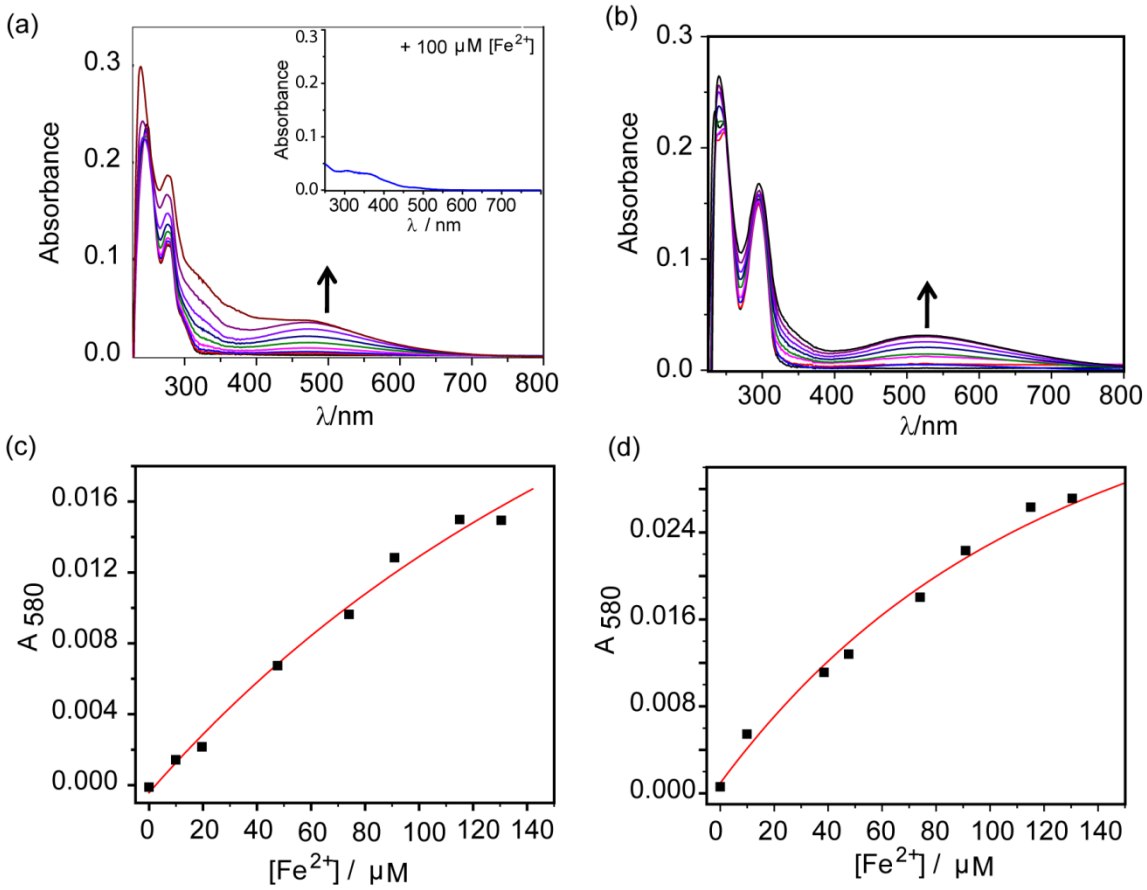

Fig. S16. Absorption titration spectra of chelators (50 µM) with increasing concentrations of Ferrous ammonium sulphate ($(NH_4)_2SO_4FeSO_4.6H_2O$). (a) Chelator **2c** with Fe^{2+} (0-150 µM); The inset shows the absorption of 100 µM Fe^{2+} salt.(b) Chelator **3c** with Fe^{2+} (0-150 µM). Final composition of the solvent was 0.2 % DMSO in deoxygenated HEPES buffer (100 mM NaCl, pH 7.0). Since the Fe^{2+} salt had minimum absorption at 580 nm, the absorbance responses of chelators (c) **2c** (d) **3c** to Fe^{2+} at 580 nm were plotted against the concentration of Fe^{2+}. The responses were fitted to a 1:1 ligand : metal binding model. The red lines represent the fits. The up arrows represent increase in absorbance intensity upon addition of metal ion.

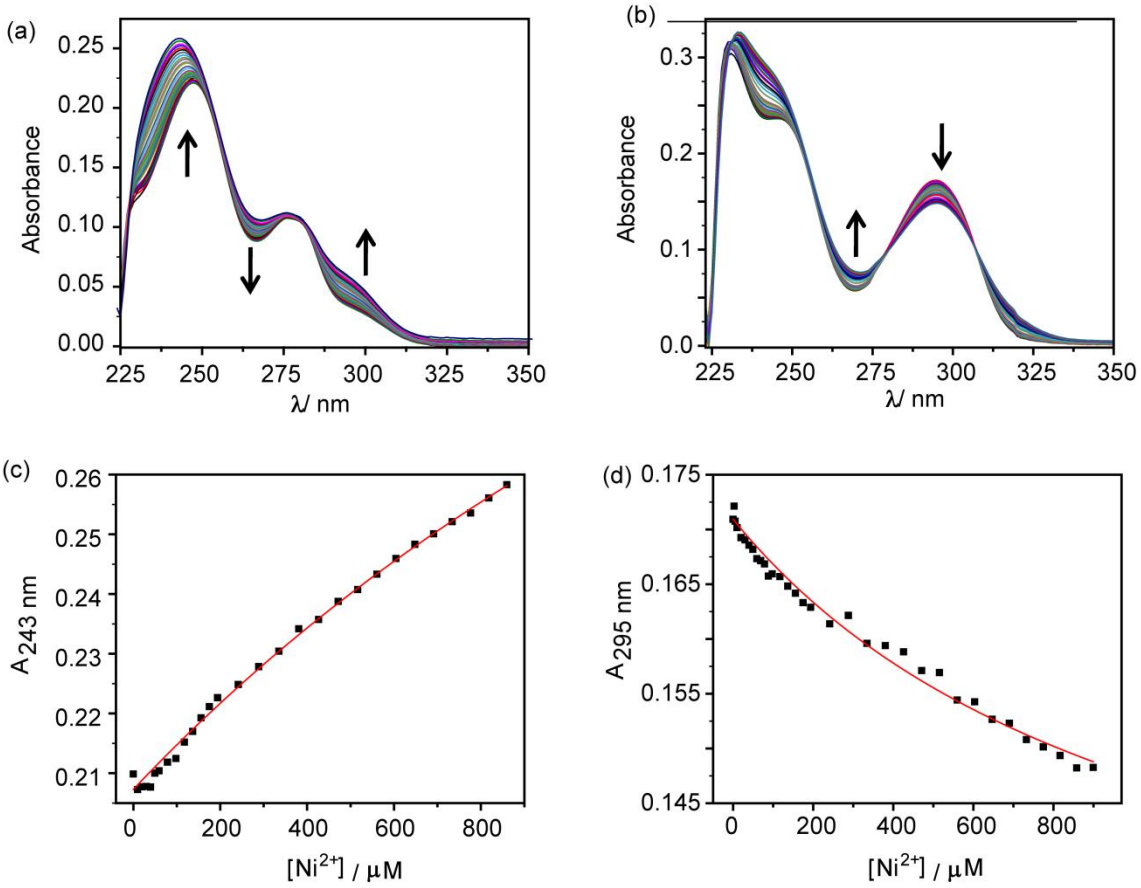

Fig. S17. Absorption titration spectra of chelators (50 μM) with increasing concentrations of $NiCl_2$. (a) Chelator **2c** with Ni^{2+} (0-1 mM); (b) Chelator **3c** with Ni^{2+} (0-1 mM) in HEPES buffer. Final composition of the solvent was 0.2 % DMSO in HEPES buffer (100 mM NaCl, pH 7.0). Absorbance at a particular wavelength was plotted with the concentration of Ni^{2+} for (c) **2c** (d) **3c** and the response was fitted to equation (1) and equation (2), respectively. The red lines represent the fits. The up and down arrows represent increase and decrease in absorbance intensity upon addition of metal ion.

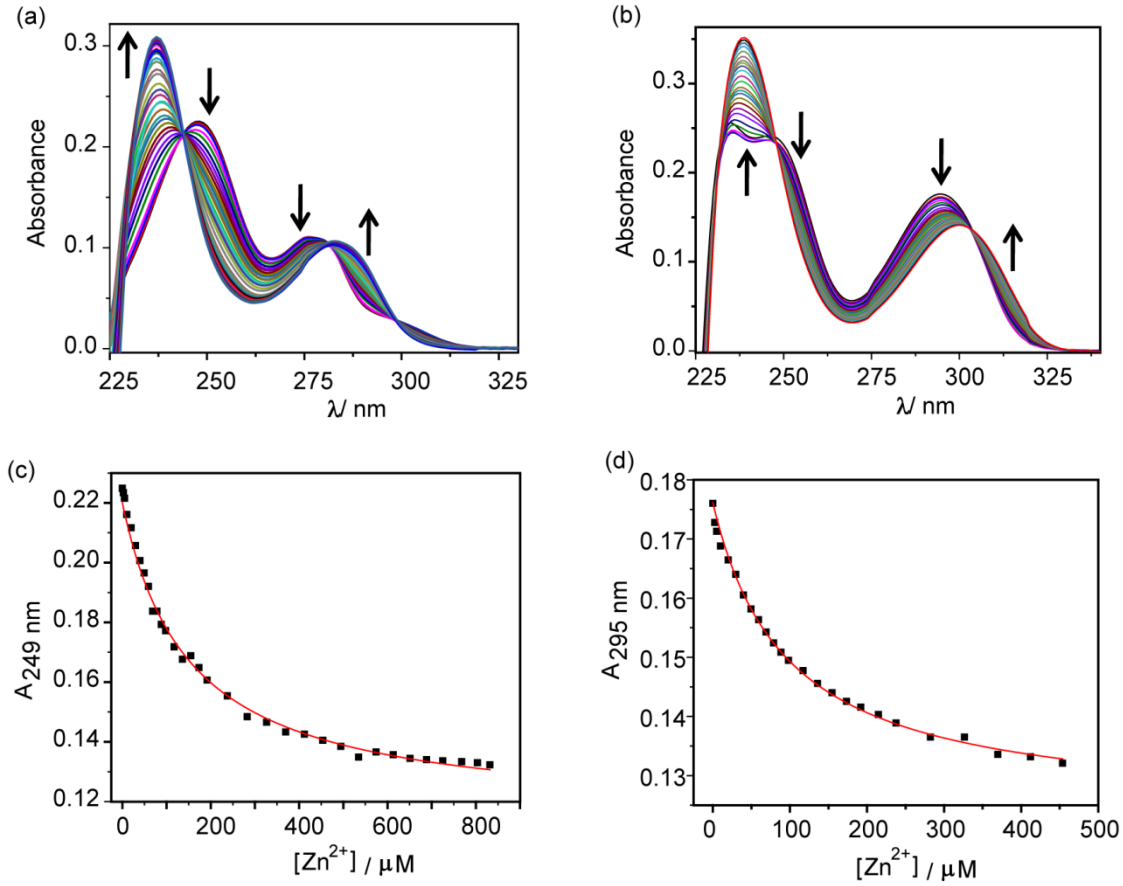

Fig. S18. Absorption titration spectra of chelators (50 µM) with increasing concentrations of $ZnCl_2$. (a) Chelator **2c** with Zn^{2+} (0-1 mM); (b) Chelator **3c** with Zn^{2+} (0-500 µM) in HEPES buffer. The final composition of the solvent was 0.2 % DMSO in HEPES buffer (100 mM NaCl, pH 7.0). Absorbance at a particular wavelength was plotted against the concentration of Zn^{2+} for (c) **2c** and (d) **3c**. The absorbance response was fitted to equation (2) and the red lines represent the fits. Up and down arrows depict increase and decrease in absorbance intensity upon addition of metal ions.

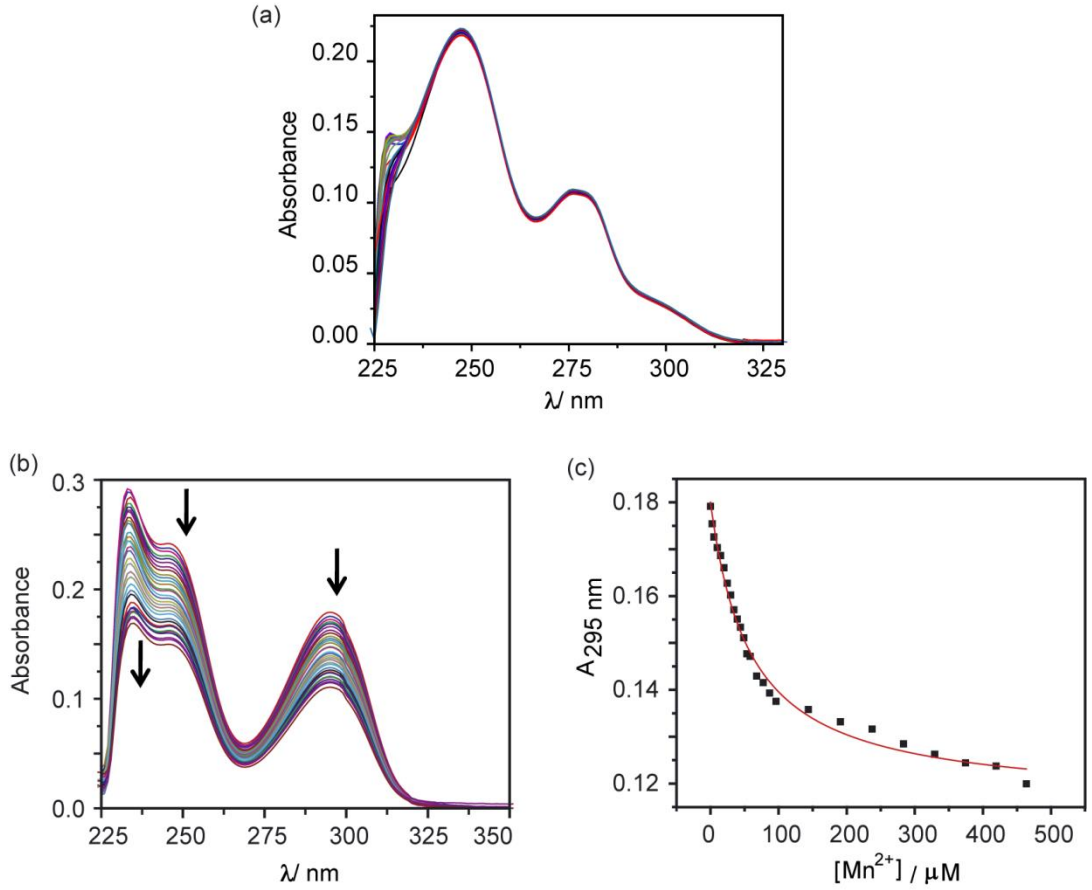

Fig. S19. Absorption titration spectra of chelators (50 µM) with increasing concentrations of $MnCl_2.4H_2O$. (a) Chelator **2c** with Mn^{2+} (0-1 mM); (b) Chelator **3c** with Mn^{2+} (0-1 mM) in HEPES buffer. The final composition of solvent was 0.2 % DMSO in HEPES buffer (100 mM NaCl, pH 7.0). (c) The absorbance response at 295 nm for chelator **3c** was fitted to equation (2) and the red line represents the fit. Down arrows indicate decrease in absorbance intensity upon addition of metal ion.

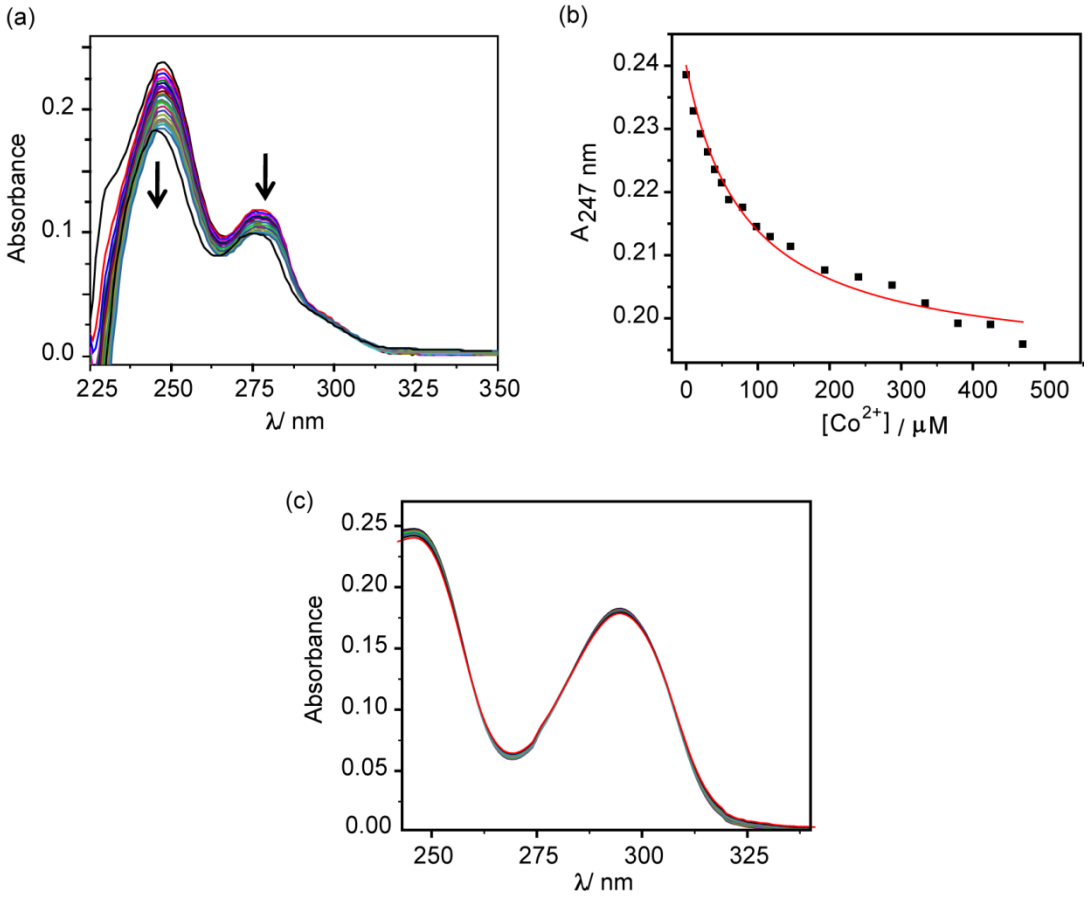

Fig. S20. Absorption titration spectra of chelators (50 μM) with increasing concentrations of $CoCl_2$. (a) Chelator **2c** with Co^{2+} (0-1 mM). (b) The absorbance response at 247 nm for **2c** was fitted to equation (2) and the red line shows the fit. (c) Absorbance titration spectra of **3c** with Co^{2+} (0-1 mM). Final composition of the solvent was 0.2 % DMSO in HEPES buffer (100 mM NaCl, pH 7.0). Down arrows indicate decrease in absorbance intensity upon addition of metal ion.

10. EPR spectrum of 2c-Cu^{2+} complex

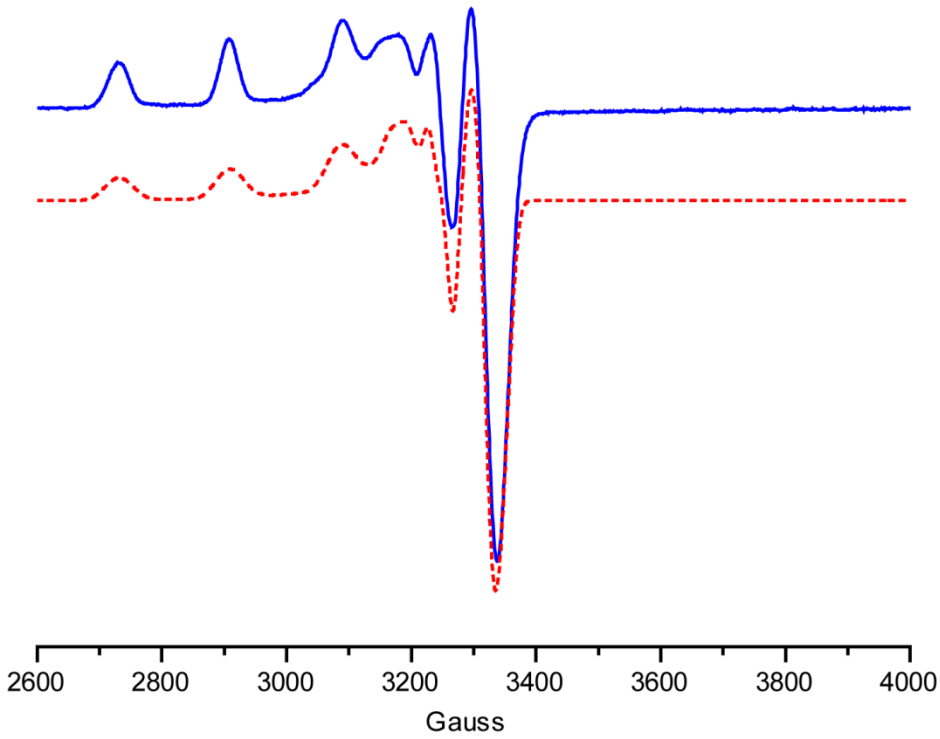

Fig. S21.Experimental X-band EPR spectrum of the **2c-Cu^{2+}** complex (solid blue line) and its EPR simulation (red dashed line). Chelator **2c** concentration was 2.2 mM, and $CuCl_2$ concentration was 1 mM in 20 mM HEPES (100 mM NaCl) with 20% glycerol at pH 7.0. The spectrum was collected on a Bruker EMX-Micro X-band EPR spectrophotometer at 87 K; microwave power: 2.37 mW; modulation amplitude: 10 G; time constant: 81.92 ms; conversion time: 100 ms; microwave frequency 9.3208 GHz. The EPR simulation was performed with the program SimFonia, using parameters g_x=g_y: 2.0502; g_z= 2.2220; A_{zz}= 177.6 G; A_{xx}= 37 G; A_{yy}= 10 G; A_N = 12.8 G, and considering 2 coordinated N atoms. $g_{\parallel}$ is greater that $g_{\perp}$ and the value of $g_{\parallel}/A_{zz}$ is 120.6 cm. These results indicate a pseudo-square planar geometry for the **2c-Cu^{2+}** complex and that no additional species (e.g. uncomplexed Cu^{2+} or dinuclear Cu^{2+} complexes) are present.

11. Absorbance response of control chelator (2-((benzylamino)methyl)phenol) with different metal ions

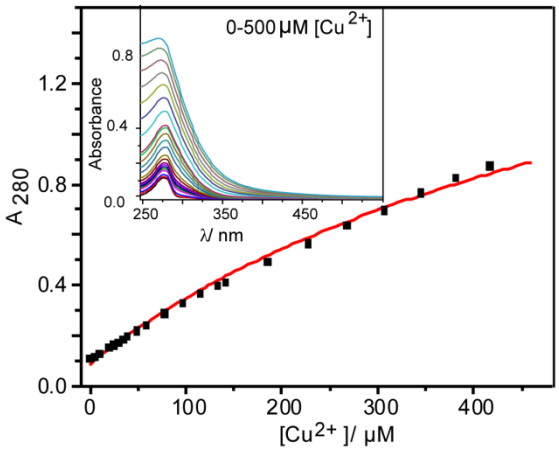

Fig. S22. Absorption titration spectra of control chelator (50 µM) with increasing concentrations of $CuCl_2$. The response at 280 nm is fitted to a 1: 2 metal:ligand binding model and red line shows the fitted plot with conditional stability constant log β of 7. The inset shows the absorption titration of chelator with Cu^{2+} (0-500 µM). Final composition of the solvent for the titration was 0.2% DMSO in HEPES buffer (100 mM NaCl, pH 7.0).

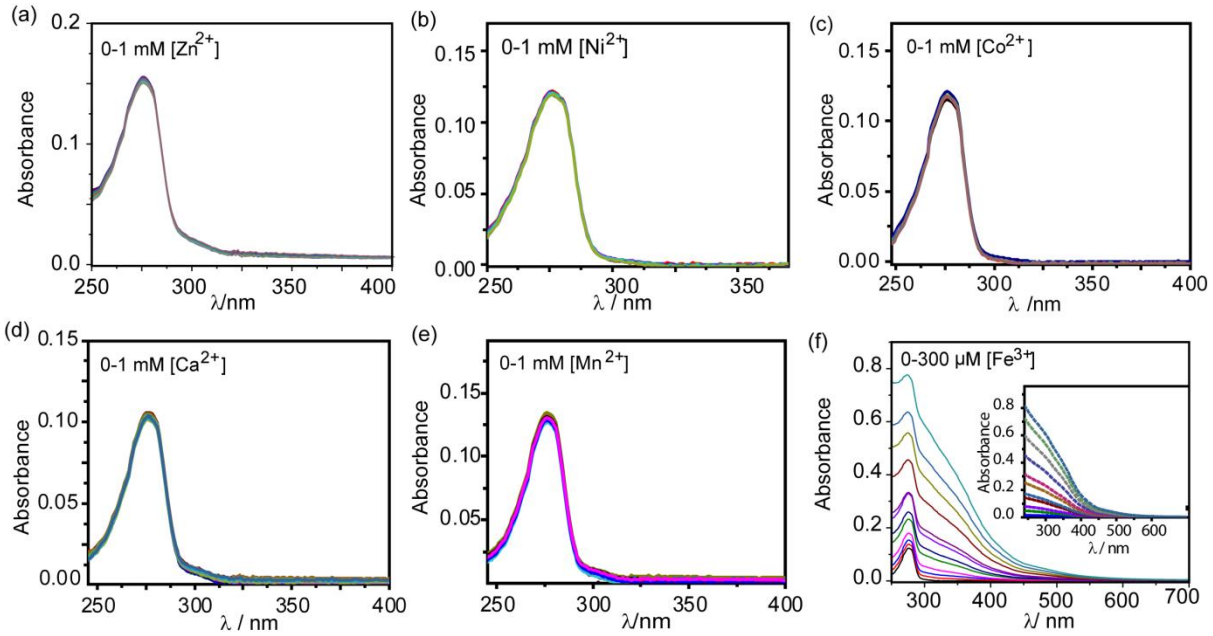

Fig. S23. Absorption titration spectra of control chelator (50 µM) with increasing concentrations of different metal ions. (a) Control chelator with $ZnCl_2$ (0-1 mM); b) Control chelator with $NiCl_2$ (0-1 mM); (c) Control chelator with $CoCl_2$ (0-1 mM); (d) Control chelator with $CaCl_2.2H_2O$ (0-1 mM); (e) Control chelator with $MnCl_2.4H_2O$ (0-1 mM); (f) Control chelator with $FeCl_3.6H_2O$ (0-300 µM); The inset shows the absorption spectra of $FeCl_3.6H_2O$ (0-300 µM) without addition of control chelator indicating that the observed rise in the absorption titration spectra in presence of ligands is due to the absorption of the iron salt and not due to binding of the chelator to Fe^{3+}. Final composition of the solvent for all titrations was 0.2% DMSO in HEPES buffer (100 mM NaCl, pH 7.0).

12. Stability constants of commercial Cu^{2+} chelators to different metal ions

Table S3: Comparison of different commercially available Cu^{2+} chelators in terms of their stability constants.

Compound	Molecular Formula	Stability Constant (log β)						Membrane Permeability
		Cu^{2+}	Zn^{2+}	Fe^{3+}	Mn^{2+}	Ni^{2+}	Co^{2+}	
[1]**EDTA**	$C_{10}H_{16}N_2O_8$	15.8	16.4	24.2	13.6	18.6	9.2	Permeable
[1]**DFO-B**	$C_{25}H_{48}O_8N_6$	14.1	11.1	30.6	-	10.9	10.3	Permeable
[1]**Trientine**	$C_6H_{18}N_4$	20.4	12.1	21.9	4.9	14.0	11.0	Permeable
[2]**8-HQ**	C_9H_7NO	25.9	18.2	26.3	13.5	20.3	18.1	Permeable
[2]**D-pen**	$C_5H_{11}NO_2S$	21.7	18.9	-	-	22.3	-	Permeable
[2]**BAL**	$C_3H_8OS_2$	17.9	23.3	30.6	10.4	22.8	-	Impermeable
[1]**Clioquinol**	C_9H_5ClINO	8.9	7	-	7.1	10.3	9.4	Permeable
Bischoline TTM	$C_{10}H_{30}MoN_2O_2S_4$	8.0	-	-	-	-	-	Permeable

Stability constant, β_{1n}= $[ML_n]/[M][L]^n$, [1]for β_{11}, [2]for β_{12} respectively; '-' No information available. Stability constant (log β) values of commonly used Cu^{2+} chelators are obtained from the literature.[4-10]

13. Stability constants of reported non-commercial reduced salen chelators to different metal ions

Table S4: Conditional stability constant (log β) of non-commercial reduced salen chelators toward different metal ions and cell-permeability.

Compound	Conditional Stability Constant (log β)						Biological Activity Studies	Membrane Permeability
	Cu^{2+}	Zn^{2+}	Fe^{3+}	Mn^{2+}	Ni^{2+}	Co^{2+}		
Salan 1	9	6	-	-	-	-	No	-
Salan 2	14.3	6.1	-	-	-	-	No	-
Salan 3	15.9	9.7	14.4	-	-	-	Yes	Permeable

Conditional stability constant, β = [ML]/[M][L]; '-' No information available. Conditional stability constant (log β) values for the reported reduced salen chelators were obtained from the literature.[9,11]

14. Deoxyribose assay protocol

The assay was performed in NaH_2PO_4 buffer (50 mM) at pH 7.4. Stock solutions (25 mM) of chelator, desferoxamine mesylate, and salicylaldehyde were prepared in DMSO. Stock solutions of $CuSO_4$ (1 mM), 2-deoxyribose (100 mM), thiobarbituric acid (TBA, 1 % w/v in 0.05 M sodium hydroxide), trichloroacetic acid (TCA, 2.8 % w/v) were freshly prepared in degassed water. Stock solutions of ascorbic acid (50 mM) and 50 % (w/w) hydrogen peroxide (10 mM) were freshly prepared in degassed buffer. In a typical constant volume experiment (final volume 0.5 mL) chelator (0-300 μM) followed by $CuSO_4$ (10 μM) were added and the mixture was stirred for 5 min. 2-deoxyribose (15 mM), H_2O_2 (100 μM) and ascorbic acid (2 mM) were added sequentially to the previous mixture. The reaction mixtures containing

increasing concentrations of the chelators were stirred for 60 min at 37 °C in dark. The solutions were allowed to cool to room temperature and the absorbance values at 532 nm were recorded. Data were plotted as A/A_0 versus chelator concentration, where A_0 and A are the absorbance at 532 nm without chelator and in presence of chelator, respectively. All measurements were carried out in triplicate, and error bars reflect standard deviation.

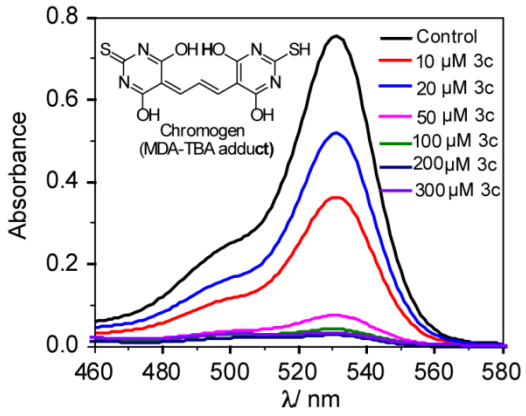

Fig. S24. Absorbance spectra of MDA-TBA adduct in NaH_2PO_4 buffer (50 mM at pH 7.4) with different concentrations of chelator **3c**.

15. Cell culture and confocal imaging protocols

Cell Culture: HEK293T and MEF cells were cultured in Dulbecco's Modified Eagle's Medium-F12 (DMEM-F12) supplemented with FBS (10 %), penicillin (50 units/mL), and streptomycin (50 μg/mL) in T25 culture flasks at 37 °C under humidified air containing 5 % CO_2. HEK293T and MEF cells were seeded on glass-bottomed dishes (35 mm diameter) coated with poly-lysine (0.1 mg/mL) and fibronectin (100 μg/mL), and cultured at 37 °C under 5 % CO_2 for 12 h, and 24 h respectively. For all experiments, a solution of either chelator **2c** or **3c** (from 25 mM stock solution in DMSO) was made in phosphate buffered saline (PBS, 20 mM $Na_2HPO_4.2H_2O$, 0.4 mM KH_2PO_4, 5.4 mM KCl, 146 mM NaCl =1X PBS) containing 5 % (w/v) glucose.

Confocal Fluorescence Imaging: All microscopy experiments were carried out at 25°C using either an LSM 880 or an LSM 710 confocal microscope (Zeiss) and images were collected in the internal detector channels using a 40X water immersion objective (Zeiss). For confocal imaging of cells Z series were obtained with a spacing of 1.00 μm. Confocal images were analyzed in ImageJ software (NIH, USA). Phen Green FL dye was used for the visualization of intracellular Cu ions. Phen Green FL dye was excited at 488 nm with a Helium-Neon laser, and emission was collected between 498 and 600 nm. Stock solutions of Phen Green FL dye (30 μM in 1X PBS buffer at pH 7.4) were prepared freshly before experiments. HEK293T cells were incubated with Phen Green FL dye (5 μM) in 1X PBS initially before any further

treatments. Each treatment with Phen Green FL (5 μM), $CuCl_2$ (20 μM), and chelator **2c** or **3c** (80 μM) were carried out for 30 min at 37 °C, under 5 % CO_2. Following each treatment, cells were thoroughly washed three times with 1X PBS. Number of washes with 1X PBS was kept identical for each set of experiments. Cells were then imaged.

CellROX® Deep Red reagent was used to detect intracellular oxidative stress. Excitation of CellROX loaded cells at 633 nm was carried out with an argon ion laser, and emission was collected between 641-700 nm. Stock solutions of CellROX (30 μM in 1X PBS buffer at pH 7.4) were prepared on weekly basis and stored at -20 °C. Control cells were incubated with CellROX (5 μM) in 1X PBS for 30 min at 37 °C under 5 % CO_2. Each treatment with $CuCl_2$ (20 μM), chelator **2c** or **3c** (40 μM), CellROX (5 μM) were carried out for 30 min at 37 °C, under 5 % CO_2. Cells were treated with CellROX for 30 min at the final step before imaging. Following each treatment, cells were thoroughly washed three times with 1X PBS and imaged.

In order to check whether the anion of the Cu^{2+} salt had any oxidative stress inducing effect, control experiments were performed by incubating HEK293T cells with $CuSO_4$. Control cells were incubated with CellROX (5 μM) in 1X PBS for 30 min at 37 °C under 5 % CO_2. Each treatment with $CuSO_4$ (20 μM), chelator **2c** or **3c** (40 μM), CellROX (5 μM) were carried out for 30 min at 37 °C, under 5 % CO_2. Cells were washed three times with 1X PBS and then imaged.

A control experiment was carried out with D-Penicillamine (D-Pen), a commercially available cell-permeable chelator in HEK293T cells. Stock solutions of D-Pen (10 mM in 1X PBS) were prepared freshly before the experiment. Control cells were incubated with CellROX (5 μM) in 1X PBS for 30 min at 37 °C, under 5 % CO_2. Each treatment with $CuCl_2$ (20 μM), D-Pen (40 μM), CellROX (5 μM) were carried out for 30 min at 37 °C, under 5 % CO_2. Following each treatment, cells were thoroughly washed three times with 1X PBS and imaged.

Lipopolysaccharide (LPS) was used to induce oxidative stress inside cells. Stock solution of LPS (1 mg/mL in water) was prepared freshly before the experiment. Cells were incubated with LPS (1 μg/mL) in 1X PBS for 30 min at 37 °C, under 5 % CO_2. Each treatment with chelator **2c** or **3c** (40 μM), and CellROX (5 μM) were carried out for 30 min at 37 °C, under 5 % CO_2. After each treatment, cells were washed three times with 1X PBS and imaged.

For simultaneous imaging of copper levels and oxidative stress in live HEK293T cells using Phen Green FL dye and CellROX dye, respectively, cells were initially incubated with Phen Green FL (5 μM) for 30 min before further treatments. Each treatment with $CuCl_2$ (20 μM), chelator **2c** or **3c** (80 μM), and CellROX (5 μM) were carried out for 30 min at 37 °C, under 5 % CO_2. Cells were incubated with CellROX (5 μM) at the final step. Following each treatment, cells were thoroughly washed three times with 1X PBS. Number of washes with 1X PBS was kept identical for each set of experiments. Cells were then imaged under confocal microscope. Z series were obtained with a spacing of 1.00 μm.

MEF wildtype (WT) and MEF Atp7a $^{-/-}$ cells were incubated with CellROX (5 μM) in 1X PBS for 30 min at 37 °C under 5 % CO_2. Cells were treated with chelator **2c** or **3c** (40 μM) for 60 min at 37 °C, under 5 % CO_2. Treatment with CellROX (5 μM) was carried out at the final step. Cells were washed with 1X PBS and then imaged.

Control experiments with Fe^{2+} salt were performed in HEK293T cells. Each treatment with Phen Green FL (5 μM), Ferrous ammonium sulphate (FAS) (20 μM), and chelator **2c** or **3c** (80 μM) were carried out for 30 min at 37 °C, under 5 % CO_2. Following each treatment, cells were thoroughly washed three times with 1X PBS. Number of washes with 1X PBS was kept identical for each set of experiments. Cells were then imaged.

In order to check whether Fe^{2+} salt had any oxidative stress inducing effect, control experiments were performed by incubating HEK293T cells with Ferrous ammonium sulphate (FAS) salt. Control cells were incubated with CellROX (5 μM) in 1X PBS for 30 min at 37 °C under 5 % CO_2. Each treatment with FAS (20 μM), chelator **2c** or **3c** (40 μM), CellROX (5 μM) were carried out for 30 min at 37 °C, under 5 % CO_2. Cells were washed three times with 1X PBS and then imaged.

16. Chelators relieve $CuSO_4$ induced oxidative stress in HEK293T cells

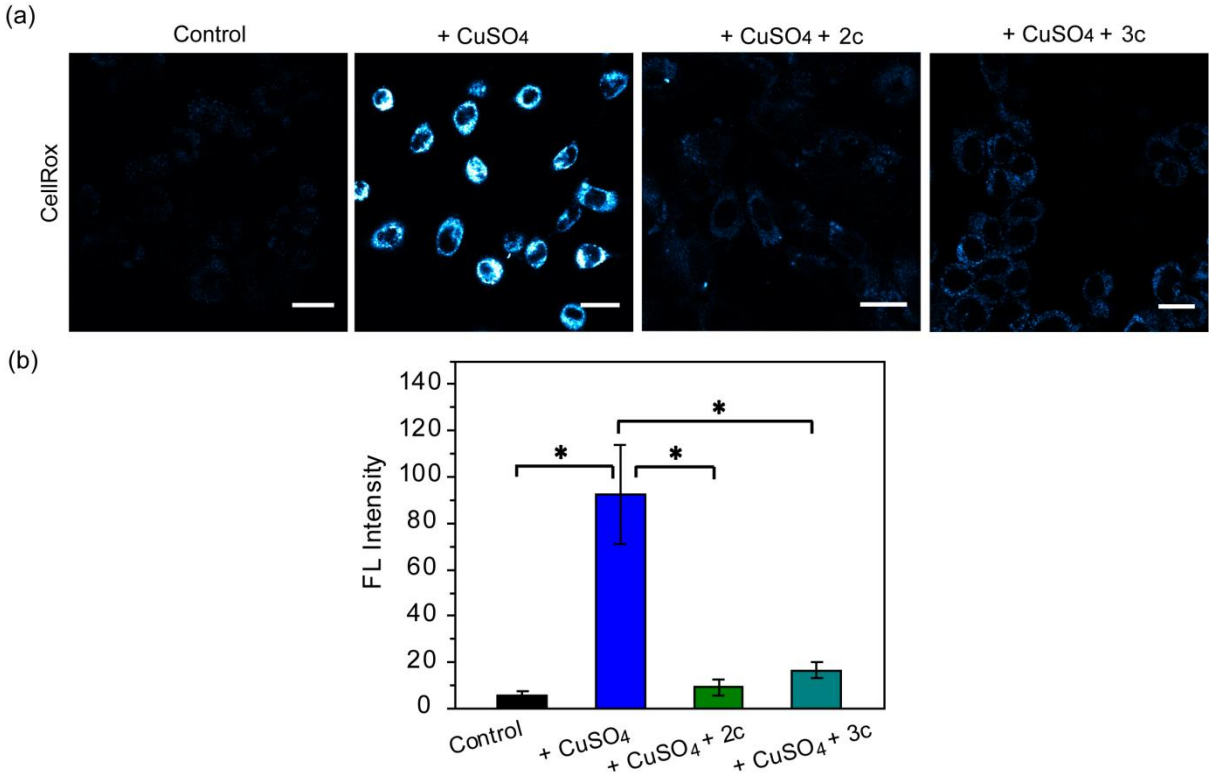

Fig. S25. Confocal fluorescence images of live HEK293T cells incubated with $CuSO_4$ and a ROS sensitive dye. (a) Left to right: control cells; cells treated with $CuSO_4$ (20 μM) for 30 min; with $CuSO_4$ (20 μM) for 30 min followed by **2c** (40 μM) for 30 min; with $CuSO_4$ (20 μM) for 30 min followed by **3c** (40 μM) for 30 min. Cells were stained with CellROX (5 μM) for 30 min at the final step before imaging. Cells were washed three times with PBS buffer after each addition and then imaged. Lower panels of (a) show bright field images of cells

overlaid with confocal images. Fluorescence intensity analyses of confocal images were performed using ImageJ software. (b) Bar plots represent the intensity analyses of confocal images. Error bars denote SEM, n = 3. Statistical analyses were performed using an unpaired, two-tailed Student's t-test (*p < 0.05). Images were acquired using a 40X objective; Scale bar: 20 µm.

17. Control experiments with chelator pre-treated cells

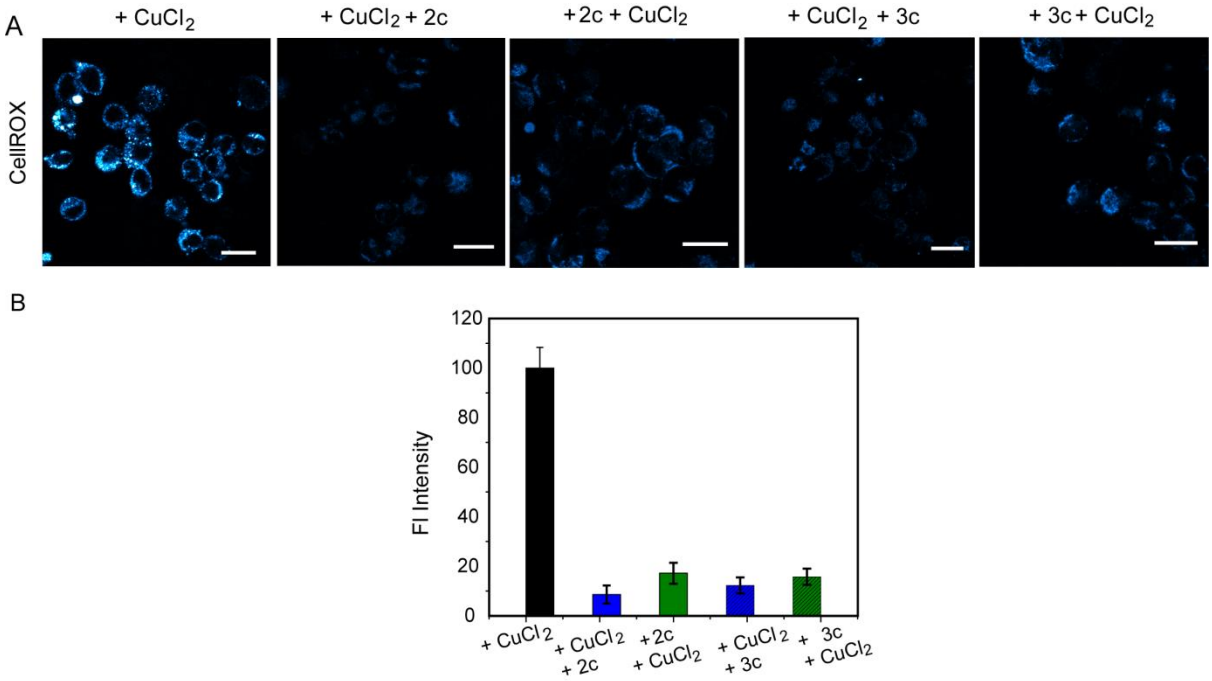

Fig. S26. Confocal fluorescence images of live HEK293T cells in presence of chelators and a ROS sensitive dye. (A) Left to right: with $CuCl_2$ (20 µM) for 30 min; with $CuCl_2$ (20 µM) for 30 min followed by chelator **2c** (40 µM) for 30 min; with chelator **2c** (40 µM) for 30 min followed by $CuCl_2$ (20 µM) for 30 min; with $CuCl_2$ (20 µM) for 30 min followed by chelator **3c** (40 µM) for 30 min, and with chelator **3c** (40 µM) for 30 min followed by $CuCl_2$ (20 µM) for 30 min. Cells were stained with CellROX (5 µM) for 30 min at the final step before imaging. Cells were washed three times with PBS buffer after each addition and then imaged. (B) Bar plots representing average fluorescence intensities obtained from intensity analysis of confocal images by using ImageJ software. Intensity data were normalized to intensity of $CuCl_2$ treated cells. Error bars denote SEM, n = 3. Images were acquired using a 40X objective; Scale bar: 20 µm.

18.Control experiments with Fe^{2+} treated cells

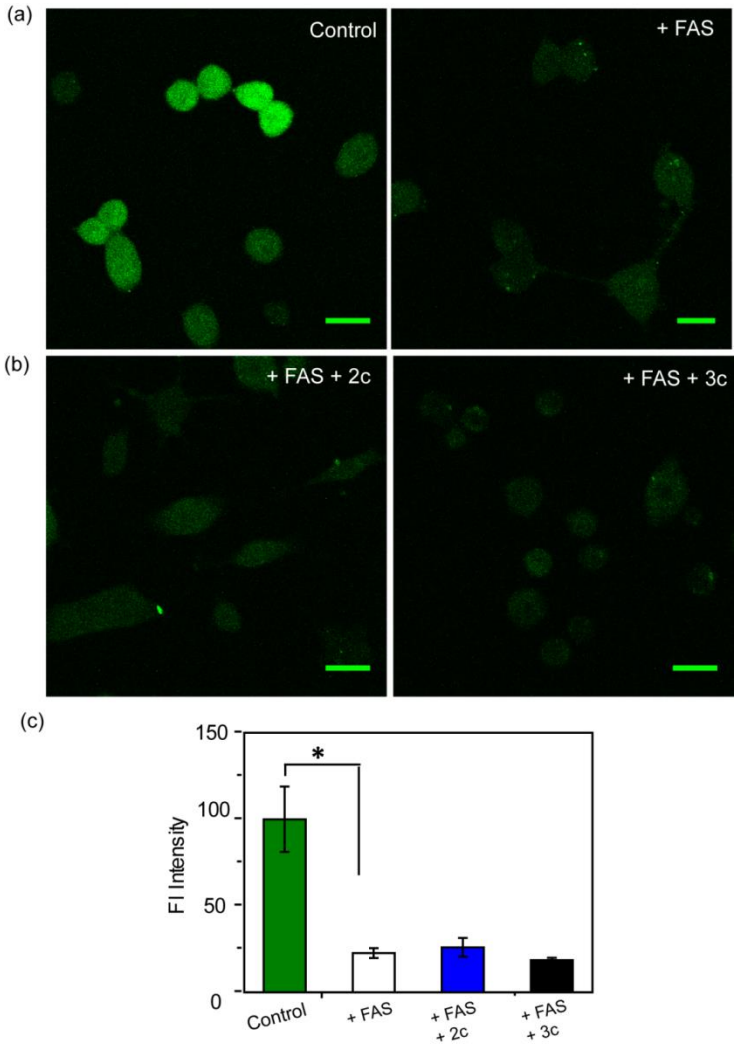

Fig. S27. Confocal fluorescence images of live HEK293T cells treated with an Fe^{2+} salt and chelators **2c** and **3c**. All cells were incubated with Phen Green FL dye (5 μM) initially for 30 min before any further treatments. (a) Left to right: control cells; cells treated with Ferrous ammonium sulphate (FAS) (20 μM) for 30 min. (b) Left to right: Cells treated with Ferrous ammonium sulphate (FAS) (20 μM) for 30 min followed by **2c** (80 μM) for 30 min; Ferrous ammonium sulphate (FAS) (20 μM) for 30 min followed by **3c** (80 μM) for 30 min. Cells were washed three times with PBS buffer after each addition and then imaged ($\lambda_{ex/em}$: 488/498−600 nm). Fluorescence intensity analyses of confocal images were carried out by using ImageJ software. (c) Bar plots represent the intensity analyses results. Intensity data were normalized to intensity of control untreated cells. Error bars denote SEM, $n = 3$. Statistical analyses were performed using an unpaired, two-tailed Student's *t*-test (*$p < 0.05$). Images were acquired using a 40X objective; Scale bar: 20 μm.

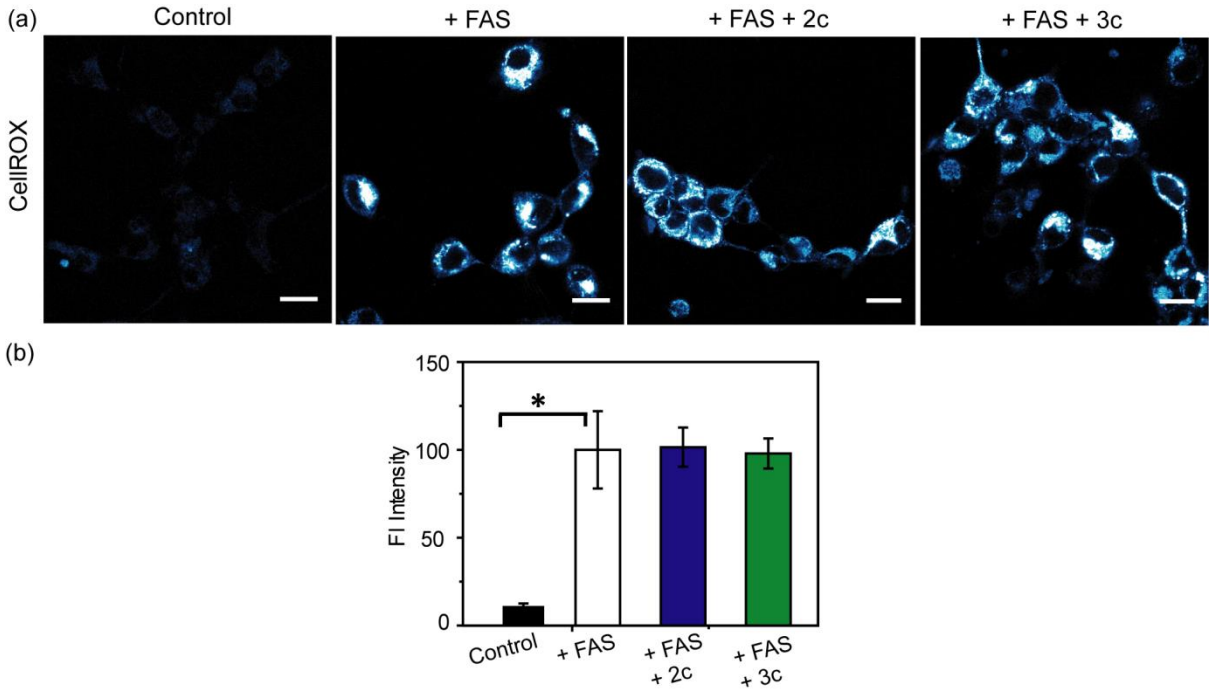

Fig. S28. Confocal fluorescence images of live HEK293T cells incubated with an Fe^{2+} salt and a ROS sensitive dye. (a) Left to right: control cells; cells treated with Ferrous ammonium sulphate (FAS, 20 µM) for 30 min; with FAS (20 µM) for 30 min followed by **2c** (40 µM) for 30 min; with FAS (20 µM) for 30 min followed by **3c** (40 µM) for 30 min. Cells were stained with CellROX (5 µM) for 30 min at the final step before imaging. Cells were washed three times with PBS buffer after each addition and then imaged. Fluorescence intensity analyses of confocal images were performed using ImageJ software. (b) Bar plots represent the intensity analyses of confocal images. Intensity data were normalized to intensity of FAS treated cells. Error bars denote SEM, $n = 3$. Statistical analyses were performed using an unpaired, two-tailed Student's *t*-test (*$p < 0.05$). Images were acquired using a 40X objective; Scale bar: 20 µm.

19. Control experiments with D-penicillamine and LPS in HEK293T cells

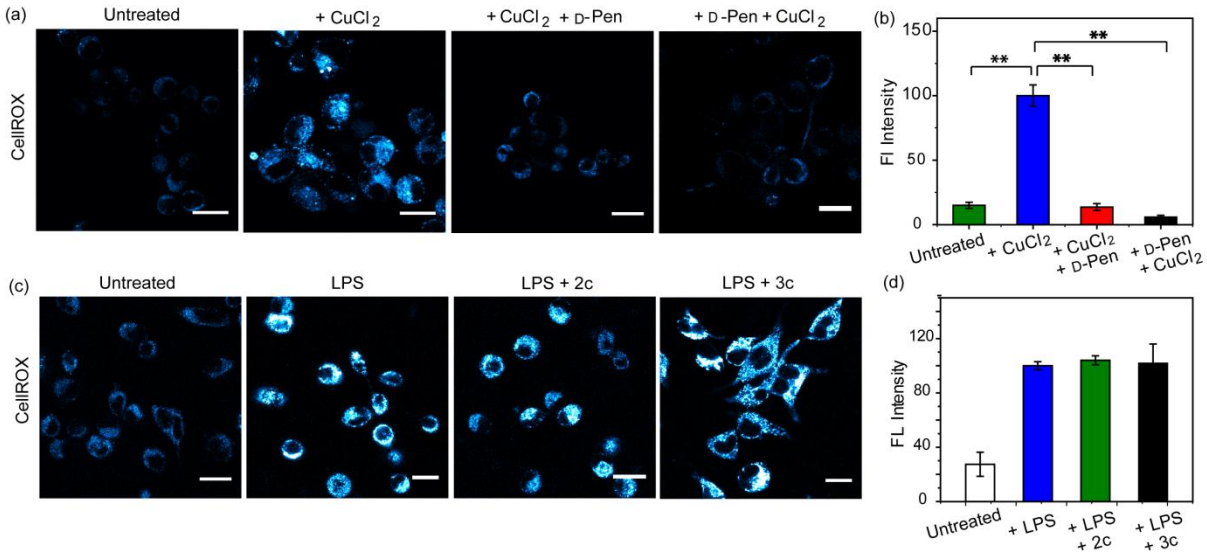

Fig. S29. (a) Confocal fluorescence images of live HEK293T cells in presence of D-Penicillamine (D-Pen) and a ROS sensitive dye, Left to right: control untreated cells; cells treated with $CuCl_2$ (20 µM) for 30 min; cells treated with $CuCl_2$ (20 µM) for 30 min followed by D-Pen (40 µM) for 30 min; cells treated with D-Pen (40 µM) for 30 min followed by $CuCl_2$ (20 µM) for 30 min. (b) Bar plots representing the intensity analyses results for panel (a). (c) Confocal fluorescence images of live HEK293T cells showing the effect of chelators **2c** and **3c** on lipopolysaccharide (LPS) treated cells. Left to right: control untreated cells; cells treated with LPS (1 µg/mL) for 30 min; with LPS (1 µg/mL) for 30 min followed by **2c** (40 µM) for 30 min; with LPS (1 µg/mL) for 30 min followed by **3c** (40 µM) for 30 min. All cells were stained with CellROX (5 µM) for 30 min in the final step. Cells were washed three times with PBS buffer after each addition, and then imaged ($\lambda_{ex/em}$: 633/641−700 nm). (d) Bar plots representing the intensity analyses results for panel (c). Intensity data were normalized to intensity of either $CuCl_2$ or LPS treated cells. Error bars denote SEM, n = 3. Statistical analyses were performed using an unpaired, two-tailed Student's t-test (**p ≤ 0.01). Images were acquired using a 40X objective; Scale bar: 20 µm.

20. Cell viability experiments

HEK293T cells were seeded into a 96 well plate and were allowed to grow until confluence was reached. For viability experiments, **2c** and **3c** were dissolved in DMSO to make stock solutions (25 mM). The stock solution was serially diluted in DMEM-F12 medium to prepare solutions containing increasing concentrations of chelators (10-200 µM). Cells were incubated with chelator solutions (100 µL) for 30 min, 2 h, 4 h, and 12 h, respectively, at 37 °C. Following incubation, cells were washed thrice with 1X PBS and treated with MTT (100 µL, 1 mg/mL) and incubated at 37 °C for 4 h. Each plate had a background control (only MTT) and a control (with cells and MTT). Acidic isopropanol solution (100 µL, 0.1 M) was added to each well and the plate was shaken well for 40 min. Absorption values at 570 nm of resultant purple formazan solutions were recorded on a microplate reader. Cell viability was calculated as follows:

% Cell viability = [(Experimental value − Background control) / (Control − Background control)] x 100.

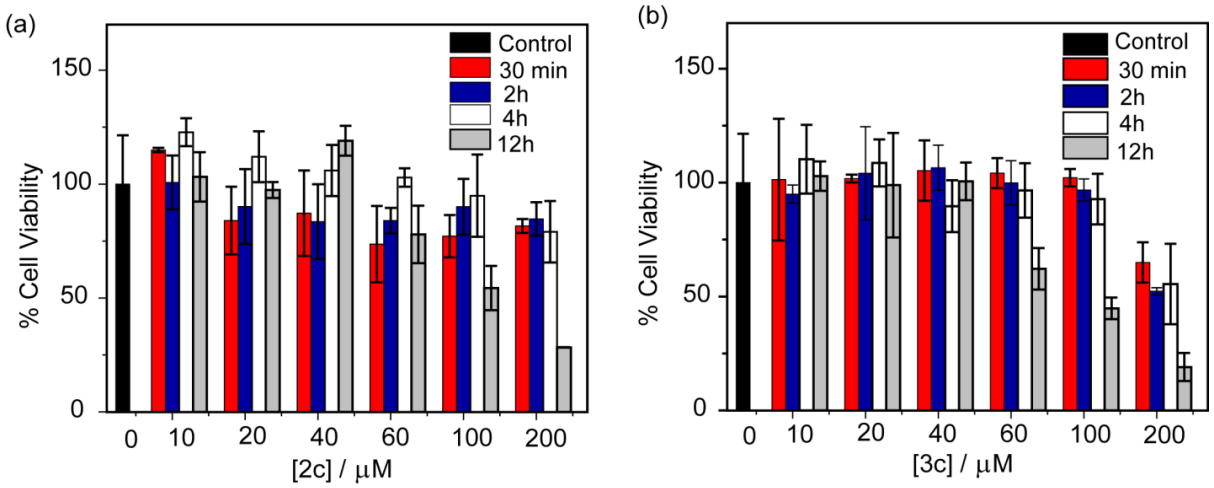

Fig. S30. Cell viability in the presence of chelators at different concentrations of (a) **2c** and (b) **3c** in HEK293T cells after 30 min, 2 h, 4 h, and 12 h of incubation. Percentage of viable cells were assessed using MTT assay. Error bars represent the SEM of three replicate experiments.

21. Western blot assay for MEF cells

Mouse embryonic fibroblast cell lysates were prepared by sonicating cell pellets in Radio immunoprecipitation assay (RIPA) lysis buffer containing Protease Inhibitor Cocktail Tablets. Whole-cell lysates (40 µg) were fractionated on 12 % SDS-PAGE and transferred onto nitrocellulose membranes. The membranes were blocked with 5 % non-fat milk in TBST and incubated in blocking buffer at 4 °C overnight with primary antibodies: rabbit anti-Atp7a and mouse anti-Tubulin. Anti-mouse or anti-rabbit horseradish peroxidase-conjugated secondary antibodies were used, and blots were developed using the SuperSignal West Pico Substrate according to the manufacturer's instructions (Pierce, Rockford, IL).

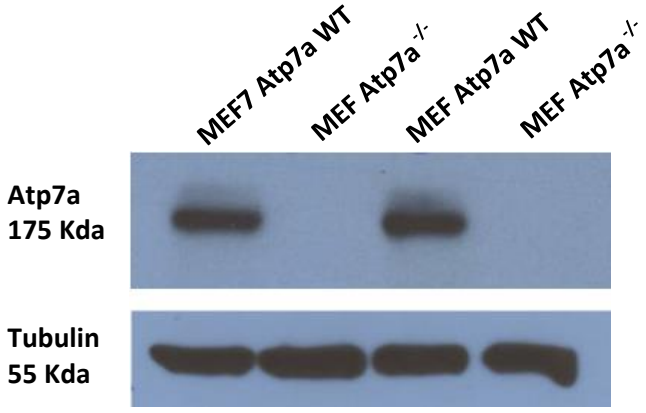

Fig. S31. Western blot gel picture showing expression levels of Atp7a (upper panel) and tubulin protein (lower panel) in MEF WT and MEF Atp7a $^{-/-}$ Cells.

22. Zebrafish imaging protocol

All experiments were performed using wildtype zebrafish larvae at 3.5 day post fertilization (dpf). Embryos were cultured at 28 °C in E3 medium containing NaCl (5 mM), KCl (170 µM), $CaCl_2$ (330 µM), and methylene blue (0.6 µM). Each treatment with $CuCl_2$ (30 µM), chelators **2c** or **3c** (60 µM), and CellROX® Deep Red (10 µM) was carried out for 30 min. Following each treatment the larvae were washed with fresh water. Each treatment with LPS (10 µg/mL), chelator **2c** (60 µM), and CellROX (10 µM) was carried out for 30 min. After each treatment, larvae were washed with water.

3.5 dpf zebrafish larvae were treated with $CuCl_2$ for 30 min followed by D-penicillamine (60 µM) for 30min. Each treatment with $CuCl_2$ (30 µM), D-penicillamine (60 µM), and CellROX (10 µM) was carried out for 30 min. After each treatment, larvae were washed with water and imaged. Confocal imaging was carried out with live anesthetized larvae using a 20X air objective (Zeiss). Zebrafish were bred and maintained following protocols approved by institutional animal ethics committee (Tata Institute of Fundamental Research).

23. Control experiments in zebrafish larvae

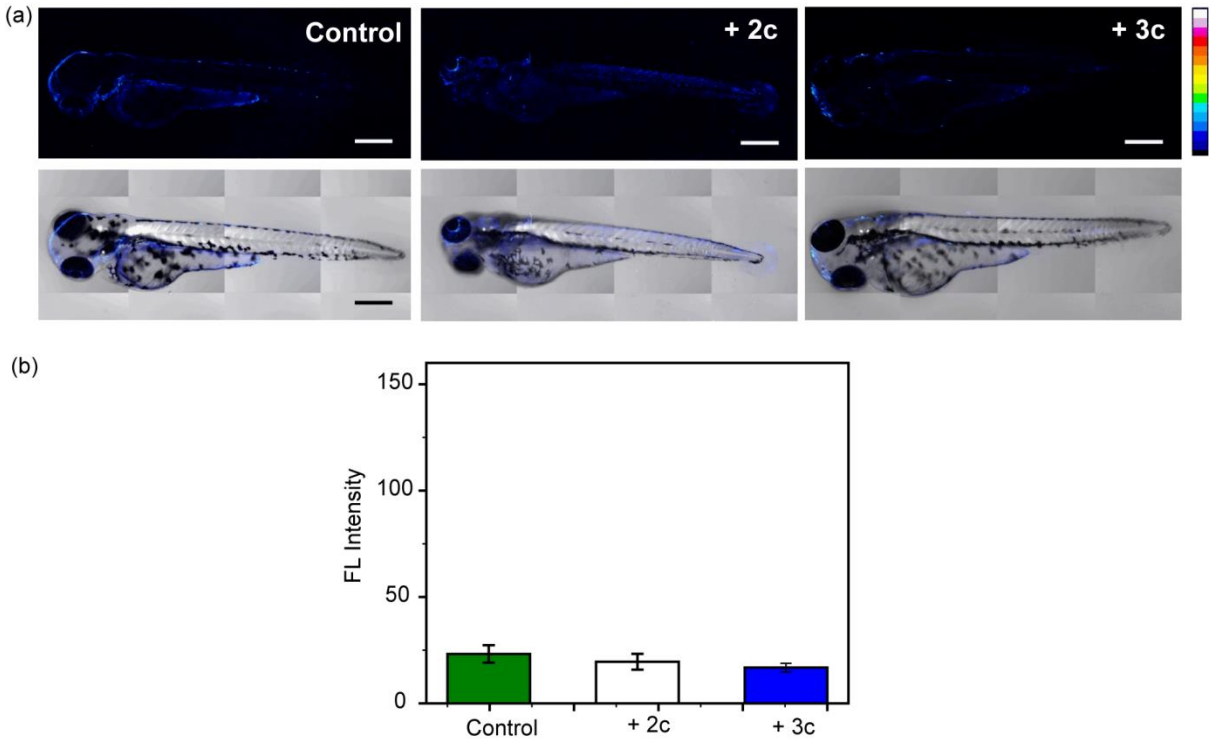

Fig. S32. Effect of chelators on 3.5 dpf zebrafish larvae in absence of added Cu ions. (a) Left to right: control untreated larvae; larvae treated with **2c** (60 µM) for 30 min; with **3c** (60 µM) for 30 min. Larvae were stained with CellROX (10 µM) for 30 min in the final step before imaging. (b) Bar plots representing average fluorescence intensities obtained from intensity analysis of confocal images of zebrafish larvae shown in panel (a) using ImageJ software. Error bars denote SEM, n = 6. 20X objective was used for imaging, Scale bar: 200 µm.

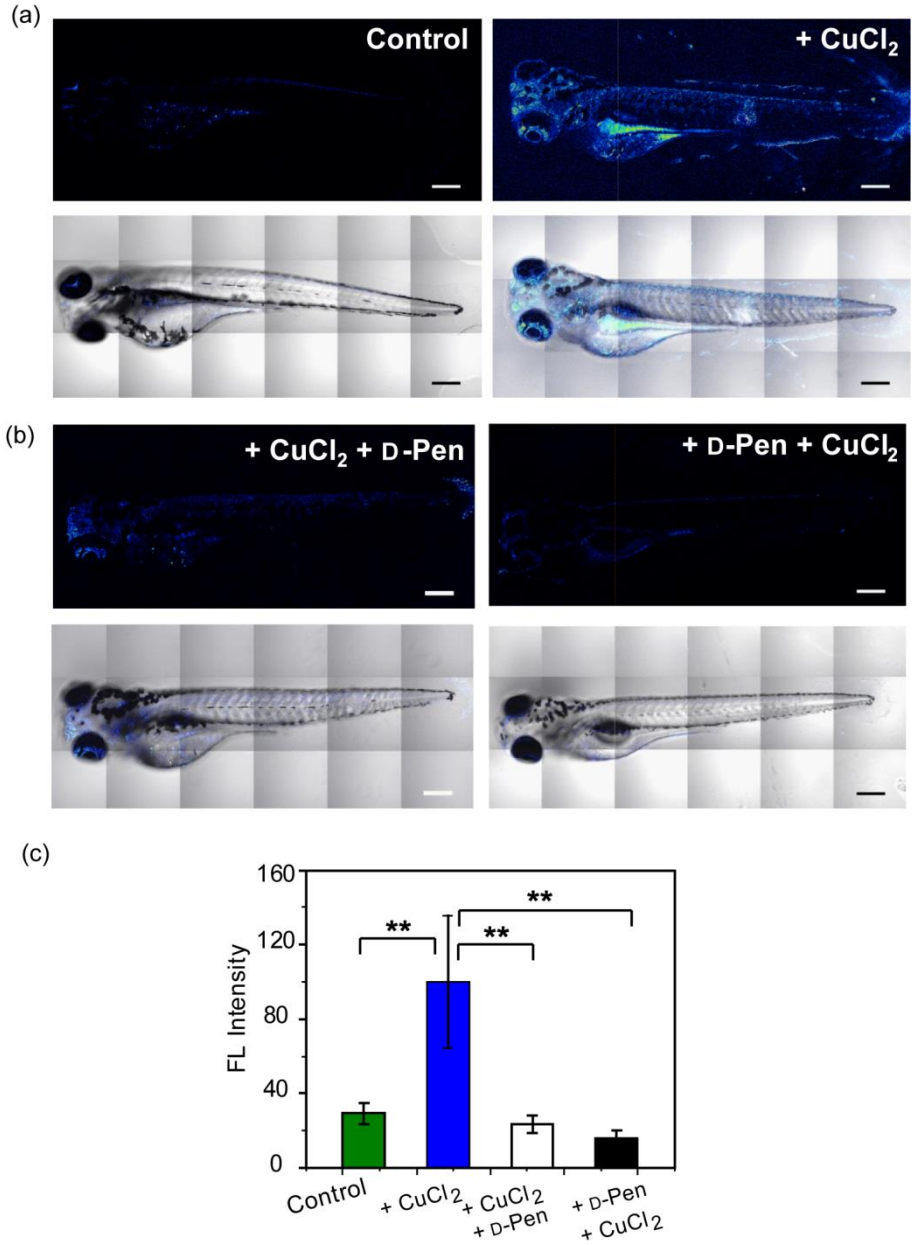

Fig. S33. Confocal fluorescence images depicting the effect of D-penicillamine (D-Pen) on live 3.5 dpf zebrafish larvae treated with $CuCl_2$. Upper panels of (a) and (b) depict Z stacked confocal fluorescence images and lower panels of (a) and (b) depict bright field images overlaid with Z stacked confocal fluorescence images. (a) Left to right: control $CuCl_2$ untreated larvae; larvae treated with $CuCl_2$ (30 μM) for 30 min. (b) Left to right: larvae treated with $CuCl_2$ (30 μM) for 30 min followed by D-Pen (60 μM) for 30 min; with D-Pen (60 μM) for 30 min followed by $CuCl_2$ (30 μM) for 30 min. Larvae were stained with CellROX (10 μM) for 30 min in the final step before imaging. (b) Bar plots representing average fluorescence intensities obtained from intensity analysis of confocal images of the zebrafish larvae using ImageJ software. The intensity data were normalized to intensity of $CuCl_2$ treated larvae. Error bars denote SEM, $n = 6$. Statistical analyses were performed using an unpaired, two-tailed Student's *t*-test (**p ≤ 0.01). 20X objective was used for imaging, Scale bar: 200 μm**.**

24. Computational studies predicting the structure of 2c-Cu^{2+} complex

We have used the established MOMEC program and force field for the structure predictions.[12-16] Additional parameters involving the bonding of phenolate O-donor atoms to Cu^{2+} were fitted to known structures (see Table S5; note that these additional parameters have not been tuned and validated on a wide experimental basis but the optimized structures, see Fig. 3, S34 and Table S6 clearly are chemically reasonable and therefore allow a thorough analysis of the ligand-induced strain in the various structures).[17,18] All Cu^{2+} centers were computed as Jahn-Teller elongated hexa-coordinate geometries with H_2O completing the coordination spheres (it may be argued that at least some of the structures might rather be 5- than 6-coordinate but this does not influence the ligand-induced strain, and hence a constant coordination number was adopted to compare the resulting strain energies). There are various possibilities to account for Jahn-Teller distortions, and all approaches are implemented in MOMEC (assignment of the Jahn-Teller axis in combination with a weaker force field parameterization for the axial bonds,[12,19] a first-order harmonic ligand field approach,[20] and ligand-field molecular mechanics[21]). Here, we have adopted the first approach.

Table S5. Force field parameters for the bonding of phenolates to Cu^{2+} added to the published MOMEC force field (k: force constant in mdyn $Å^{-1}$ or mdyn rad^{-1}; p^o: equilibrium distance or angle or off-set angle in Å or rad; in general, torsions and out-of-plane functions involving the metal center are not included; Van der Waals interactions with the metal center have not been parameterized, see main text).[13-16]

	k	**P^o**
Cu-O	0.800	1.900
O-C	6.500	1.340
C-C-O	0.970	2.094
L-Cu-O^{eq}	0.013	1.571
L-Cu-O^{ax}	0.007	1.571
Cu-O-C	0.200	2.094
-O-C-	0.050	1.571 (mult: 6.0)

We have optimized possible [Cu (**2c**)]$^{n+}$ complexes with Cu:ligand = 1:1 stoichiometry, and **2c** as a bi, tri-, tetra- or penta-dentate ligand, to get comparable strain energies. 1:2 (and 2:1) complexes were not considered initially. We note that not all possible configurational isomers were optimized (i.e. not all possible facial vs. meridional configurations of 3-, 4- and 5-dentate ligands); also a full conformational analysis was not performed. Both would have been possible, e.g. with Monte Carlo

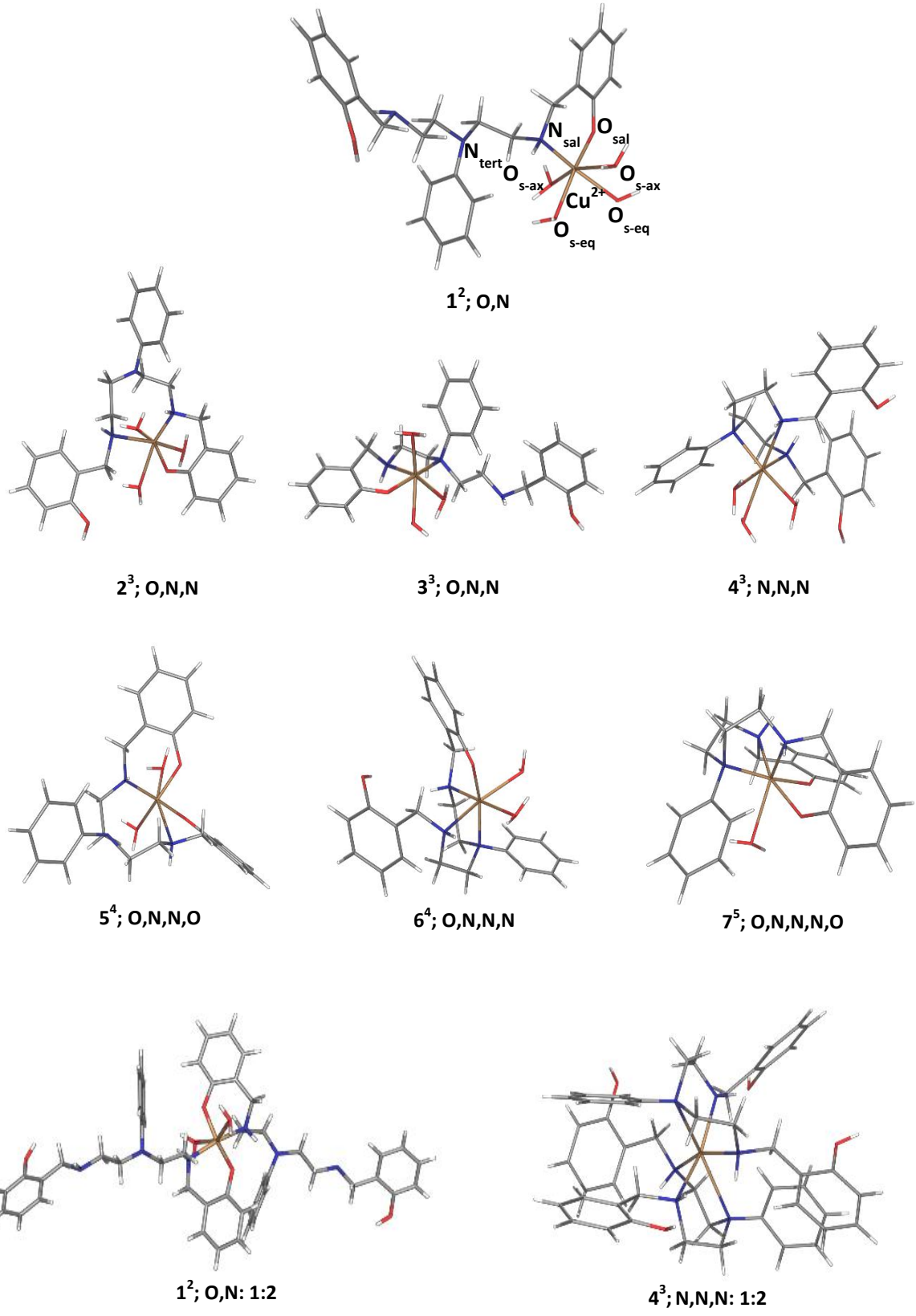

Fig. S34. MOMEC optimized structures of $[Cu(\mathbf{2c})]^{n+}$ complexes. Computed structures with labels used in Tables S6 (see also Fig. 3) and specification of the donor sets as used in the text above and in the manuscript. In these structures, carbon, nitrogen, oxygen, and hydrogen atoms are represented in grey, blue, red and white color, respectively. Copper ions are represented in gold.

type modules, available in MOMEC[22]; however, such a time-consuming analysis would not have led to additional insight. The analysis presented in Fig. S34, Tables S6 and S7 is based on a semi-deterministic construction of the most relevant isomers and therefore assembles the most relevant structures based on coordination of **2c** (or **3c**) to Cu^{2+}.

From Table S6, it emerges that the only energetically relevant structures with 1:1 stoichiometry are 1^2 (O,N), 5^4 (O,N,N,O) and 2^3 (O,N,N), which all are in a margin of 15 kJ/mol. All other structures are more than approximately 25 kJ/mol higher in energy than 1^2. Interestingly, all three low energy structures have the central, phenyl-substituted tertiary amine N_{tert} not coordinated to Cu^{2+}, suggesting that this is the reason for their lower energy, and this is primarily due to an increase of the Van der Waals term (approximately 40 kJ/mol versus approximately 20 kJ/mol), when N_{tert} is coordinated. A careful inspection of the optimized structures and the corresponding individual strain energy terms shows that this is primarily due to the *-N_{tert}-C_{phen}-* torsional angles, which are enforced to around 30° upon coordination of N_{tert} to Cu^{2+}. In the favored conformation where N_{tert} is uncoordinated as in the metal-free ligand, this torsional angle is around 90° (see structure 1^2 (1:2)). With N_{tert} coordinated, one of the α-hydrogen atoms of the phenyl substituent points directly to the metal center (note that the MOMEC force field – as other force fields – generally does not consider Van der Waals repulsion with the metal center[23], and the *-N_{tert}-C_{phen}-* torsion has been fixed as outlined above with a large damping during the optimization process, i.e. without artificial constraints). While this prevents the H···Cu^{2+} repulsion, it leads to severe intra-ligand H···H repulsion.

Table S6. Total strain, bond stretching, angle bending, torsional strain, and Van der Waals repulsion energies for the nine computed structures depicted in Fig. S34.

kJ mol^{-1}	1^2	1^2 (1:2)	2^3	3^3	4^3	4^3 (1:2)	5^4	6^4	7^5
E_{total}	58.13	129.71	73.42	82.86	82.65	175.88	69.18	89.41	109.95
E_{bond}	3.53	8.32	4.90	7.76	7.73	24.94	4.90	7.34	12.19
E_{angle}	20.56	40.19	23.59	18.58	22.94	60.83	26.30	24.31	35.25
$E_{torsion}$	13.27	29.24	21.58	17.89	10.42	26.67	13.90	16.67	17.02
E_{vdw}	20.77	51.97	23.35	38.63	41.55	63.44	24.08	41.09	45.49

The other two low energy structures (5^4 (O,N,N,O) and 2^3 (O,N,N)) both have an 8-membered chelate ring involving the uncoordinated phenyl-substituted amine N_{tert}. Clearly, this leads to structures with very unfavorable entropy terms and, therefore, 1^2 (O,N) is the only stable structure, i.e. 1:2 metal:ligand coordination with each ligand in a 1^2 coordination mode (see Fig. 3b and Supporting Video) is the favored structure, and this is in agreement with the observed electronic spectra (CT and d-d transitions, respectively at 420 and 623 nm, see manuscript), the spectrophotometric titration, EPR

spectrum, and ESI-MS data. Note that species where two ligand molecules of either **2c** or **3c** are coordinated to one Cu^{2+} center with different coordination modes are also possible but, given the clear isosbestic points and the spectroscopic data, this is rather unlikely.

Table S7. Optimized Cu^{2+}-donor distances for the nine structures shown in Fig. S34.
(Jahn-Teller elongated bonds in italics; nomenclature as in Fig. S34 and Table S6).

Distances in Å	**1^2**	**1^2 (1:2)**	**2^3**	**3^3**	**4^3**	**4^3 (1:2)**	**5^4**	**6^4**	**7^5**
Cu-O_{sal}	1.89	1.90 1.92	1.90	1.92			1.93 1.92	1.92	1.99 1.97
Cu-N_{sal}	1.95	1.99 1.98	1.95 *2.64*	2.03	1.99 *2.45*	2.09 2.11 2.09 2.11	2.00 *2.59*	1.98 *2.53*	2.08 *2.40*
Cu-N_{tert}				2.02	2.05	*2.75* *2.76*		2.05	2.09
Cu-$O_{s\text{-}eq}$	2.19 2.29		2.27 2.32	2.29	2.24 2.26		2.36	2.27	
Cu-$O_{s\text{-}ax}$	*2.55* *2.52*	*2.73* *2.63*	*2.56*	*2.58* *2.59*	*2.54*		*2.66*	*2.55*	*2.57*

25. ^{1}H NMR and ^{13}C NMR spectra

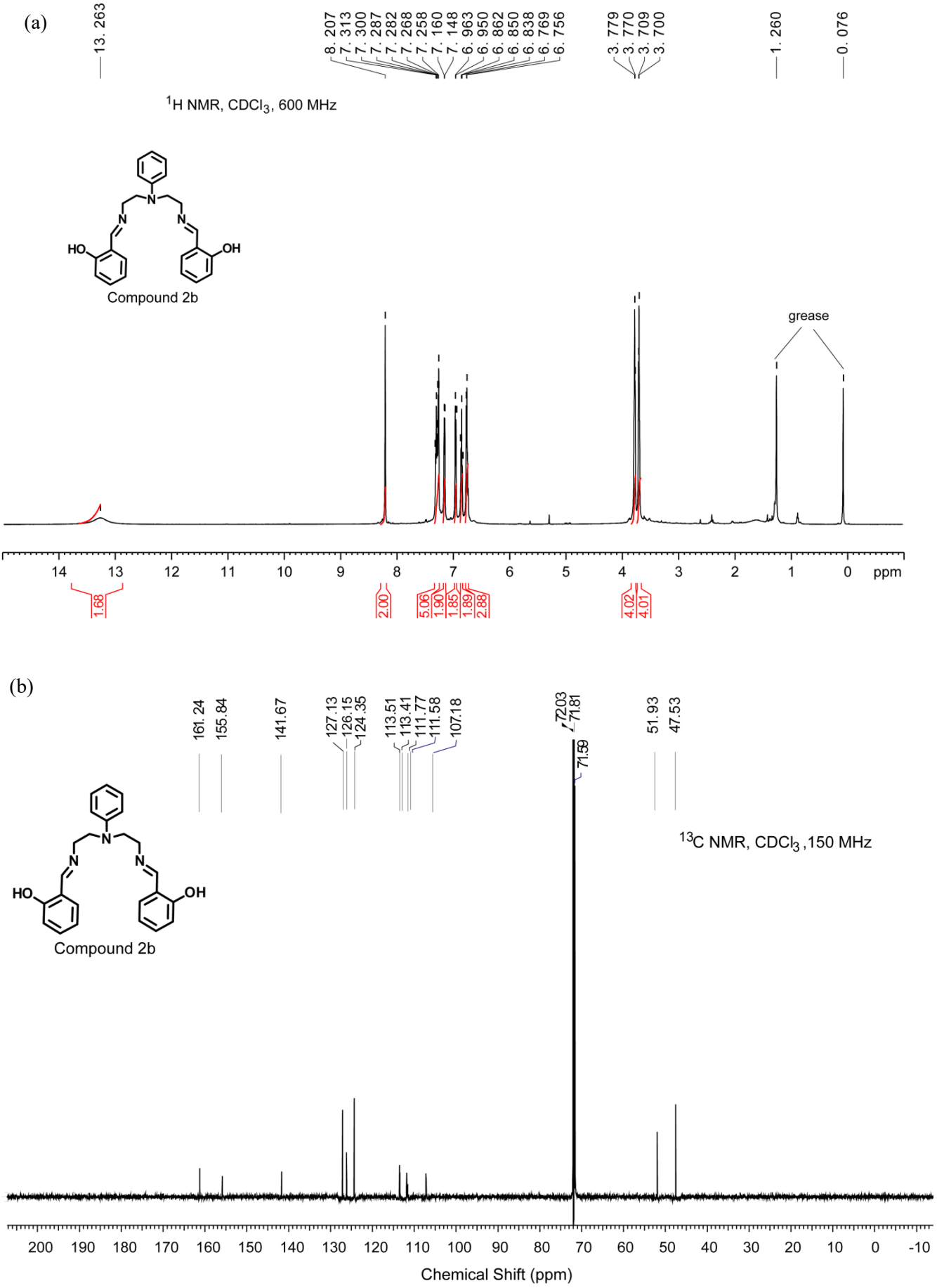

Fig. S35. (a) ^{1}H NMR and (b) ^{13}C NMR of compound **2b** at 25°C in $CDCl_3$.

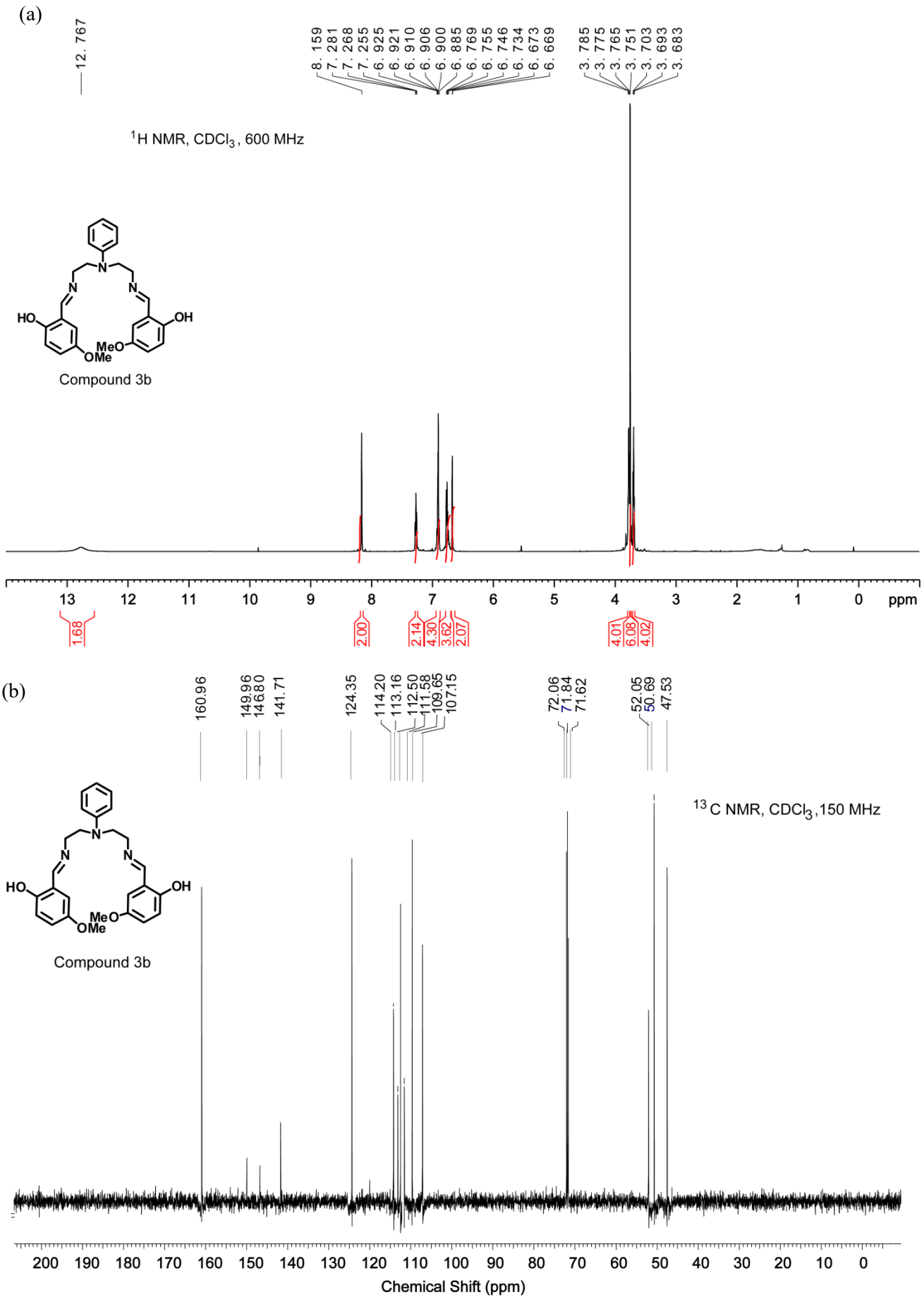

Fig. S36. (a) ^{1}H NMR and (b) ^{13}C NMR of compound **3b** at 25°C in $CDCl_3$.

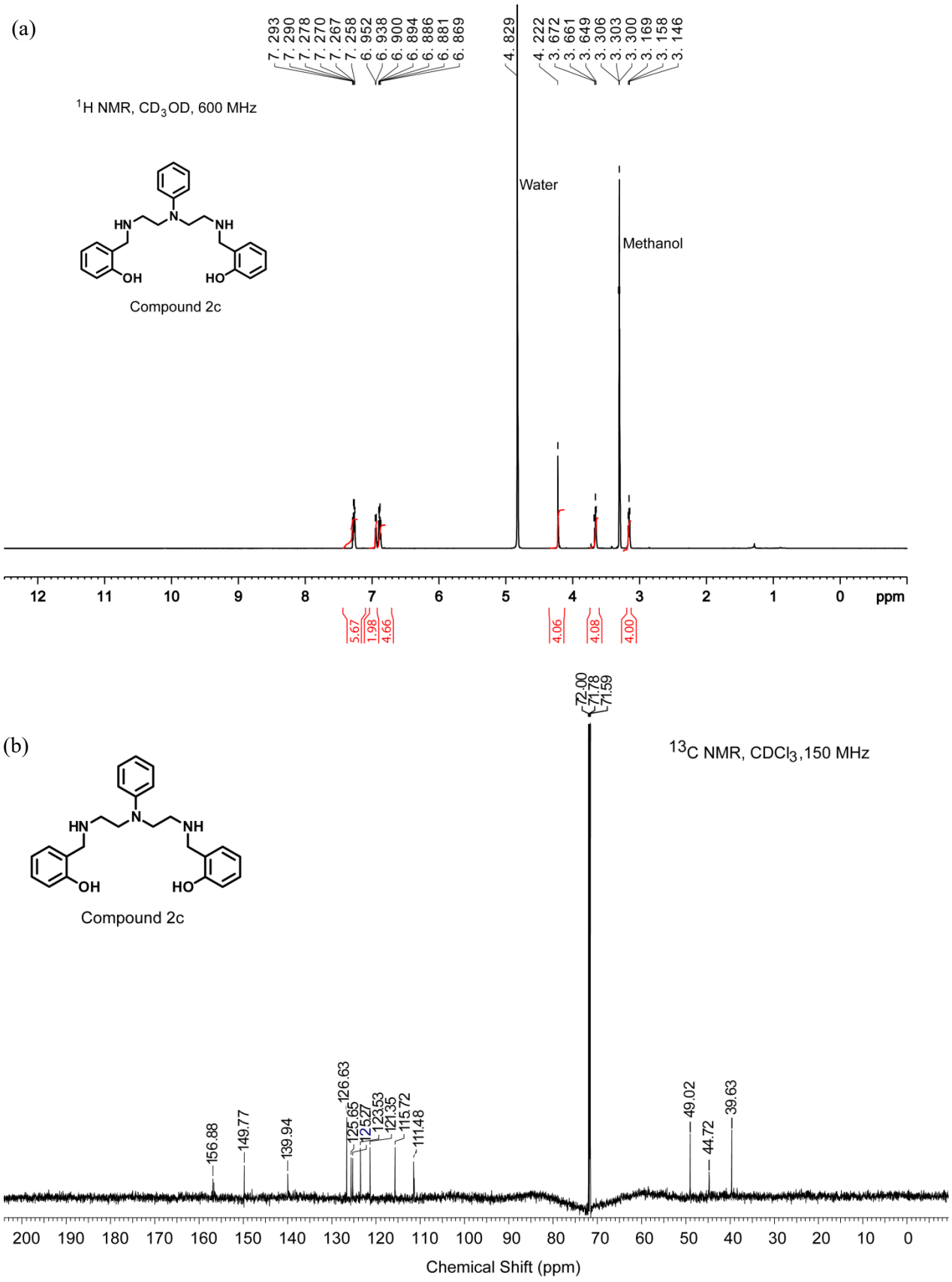

Fig. S37. (a) ^{1}H NMR and (b) ^{13}C NMR of compound **2c** at 25°C in CD_3OD and $CDCl_3$, respectively.

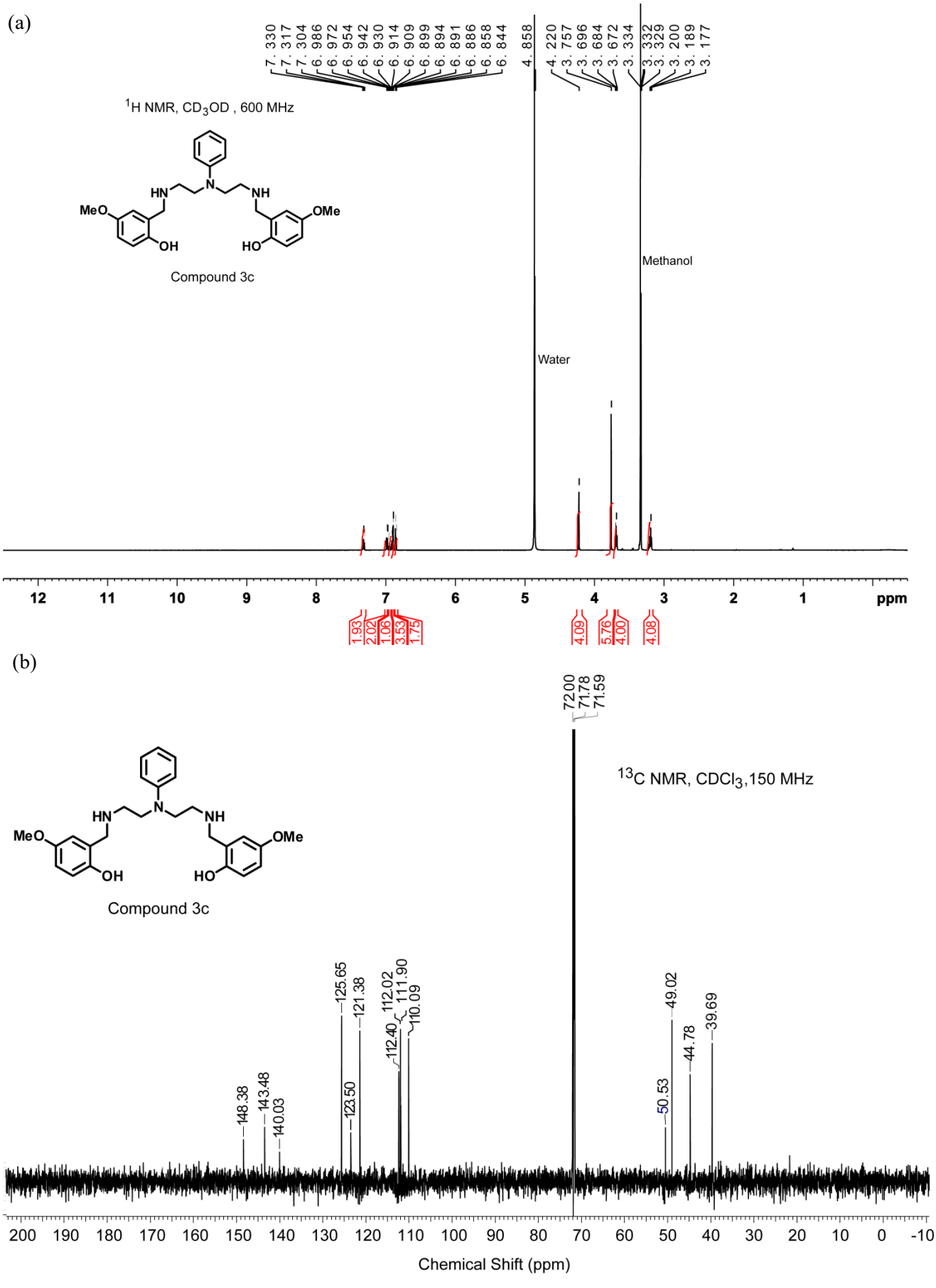

Fig. S38. (a) (a) ^{1}H NMR and (b) ^{13}C NMR of compound **3c** at 25°C in CD_3OD and $CDCl_3$, respectively.

26. References

(1) Lee, S. J.; Lee, S. S.; Lee, J. Y.; Jung, J. H. *Chem. Mater.* **2006**, *18*, 4713.
(2) Harry, K.; Spivack, J. D.; Patent US2928876: 1960.
(3) Sathiyaraj, E.; Thirumaran, S.; Selvanayagam, S.; Sridhar, B.; Ciattini, S. *J. Mol. Struct.* **2018**, *1159*, 156.
(4) Sillen, L. G., Martell, A.E., *Stability Constants of Metal Ion Complexes, Chemical Society*; 17 ed., **1964**.
(5) Ding, X.; Xie, H.; Kang, Y. J. *J. Nutr. Biochem.* **2011**, *22*, 301.
(6) Juarez, J. C.; Betancourt, O.; Pirie-Shepherd, S. R.; Guan, X.; Price, M. L.; Shaw, D. E.; Mazar, A. P.; Doñate, F. *Clin. Cancer Res.* **2006**, *12*, 4974.
(7) Kuchinskas, E. J.; Rosen, Y. *Arch. Biochem. Biophys.* **1962**, *97*, 370.
(8) Sillen, L. G., Martell, A.E., *Stability Constants, Supplement No 1, Alden Press, Oxford* **1971**.
(9) Leed, M. G. D.; Wolkow, N.; Pham, D. M.; Daniel, C. L.; Dunaief, J. L.; Franz, K. J. *J. Inorg. Biochem.* **2011**, *105*, 1161.
(10) Budimir, A.; Humbert, N.; Elhabiri, M.; Osinska, I.; Birus, M.; Albrecht-Gary, A. M. *J. Inorg. Biochem.* **2011**, *105*, 490.
(11) Robert, A.; Liu, Y.; Nguyen, M.; Meunier, B. *Acc. Chem. Res.* **2015**, *48*, 1332.
(12) Comba, P.; Hambley, T. W.; Martin, B. In *Molecular Modeling of Inorganic Compounds, 3rd Edition with a Tutorial, based on MOMEC3*; Wiley-VCH Verlag GmbH & Co. KGaA: **2009**, p 215.
(13) Bernhardt, P. V.; Comba, P. *Inorg. Chem.* **1992**, *31*, 2638.
(14) Comba, P.; Ströhle, M.; Hambley, T. W. *Helv. Chim. Acta* **1995**, *78*, 2042.
(15) Bol, J. E.; Buning, C.; Comba, P.; Reedijk, J.; Ströhle, M. *J. Comput. Chem.* **1998**, *19*, 512.
(16) Comba, P.; Martin, B.; Sanyal, A. *J. Comput. Chem.* **2013**, *34*, 1598.
(17) Ebrahimipour, S. Y.; Sheikhshoaie, I.; Castro, J.; Haase, W.; Mohamadi, M.; Foro, S.; Sheikhshoaie, M.; Esmaeili-Mahani, S. *Inorganica Chim. Acta.* **2015**, *430*, 245.
(18) Tarnai, M. *PhD Thesis, Heidelberg University* **2006**.
(19) Comba, P.; Remenyi, R. *Coord. Chem. Rev.* **2003**, *238*, 9.
(20) Comba, P.; Zimmer, M. *Inorg. Chem.* **1994**, *33*, 5368.
(21) Bentz, A.; Comba, P.; Deeth, R. J.; Kerscher, M.; Seibold, B.; Wadepohl, H. *Inorg. Chem.* **2008**, *47*, 9518.
(22) Bartol, J.; Comba, P.; Melter, M.; Zimmer, M. *J. Comput. Chem.* **1999**, *20*, 1549.
(23) Hambley, T. W.; Jones, A. R. *Coord. Chem. Rev.* **2001**, *212*, 35.